Rare-Earth Transition-Metal Chalcogenides

Kwasi Mitchell and James A. Ibers*

Department of Chemistry, Northwestern University, 2145 Sheridan Road, Evanston, Illinois 60208

Received November 19, 2001

Contents

10.1021/cr010319h CCC: $39.75
Published on Web 05/03/2002

I. Introduction

Metal chalcogenides are characterized generally by the absence of closest packing and the propensity for Q···Q interactions (Q = S, Se, Te). As a consequence, low-dimensionality and anisotropic physical properties often result. Interest in metal chalcogenides stems not only from their structures but from the variety of physical properties that they exhibit. These include low-temperature superconductivity,[1] charge-density waves,[2] optical properties,[3,4] and thermoelectricity.[5]

A subset of metal chalcogenides, namely, rare-earth transition-metal chalcogenides, is the subject of this review. These compounds, which contain a combination of d- and f-elements, are of fundamental interest in solid-state chemistry and materials science; in addition, there is the potential for useful physical properties. The 3d metals, in particular Fe, Co, and Ni, are strong itinerant electron ferromagnets, whereas the lanthanides have localized 4f moments with high anisotropic energy. Thus, the magnetic exchange energy in 3d/4f compounds may comprise three different types of spin−spin interactions, namely 3d−3d, 3d−4f, and 4f−4f, to give materials suitable for magnetic storage.[6,7] Additionally, d-element chalcogenide semiconductors, such as MQ (M = Zn, Cd), are widely used for their optical properties.[8] Traditional chalcogenide luminescent materials of this type have been doped with Cu^+, Ag^+, Mn^{2+}, Ln^{3+}, or other cations to produce diluted magnetic semiconductors with modified luminescent and magnetic proper-

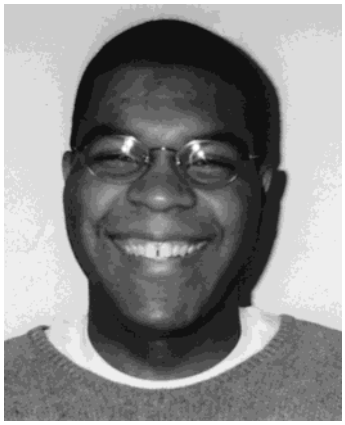

Kwasi Mitchell was born in Kalamazoo, MI, in 1977. He graduated *cum laude* with his B.A. degree in Chemistry at Kalamazoo College (1999). Kwasi is currently a Ford Foundation predoctoral fellow in the Department of Chemistry at Northwestern University. His research topics include the high-temperature solid-state preparation and characterization of 3d–4f chalcogenide magnetic semiconductors.

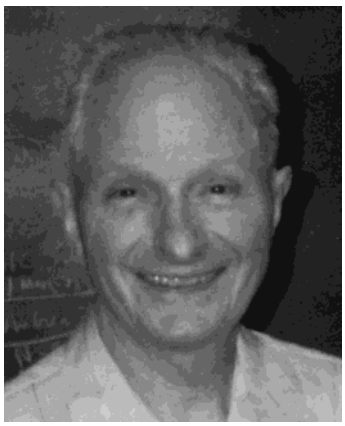

James A. Ibers was born in Los Angeles in 1930. He received his Ph.D. degree from Caltech in 1954. After a period in industry and at Brookhaven he became Professor of Chemistry at Northwestern University in 1964. His research interests include the solution and solid-state chemistry of metal chalcogenides.

ties.[3,9] Examples of 3d/4f compounds, albeit not chalcogenides, with interesting properties include the industrially important materials Nd:YIG[10] and the permanent magnetic alloys $SmCo_5$ and $Nd_2Fe_{14}B$[11] as well as the heavy fermion conductors $CeRu_2Si_2$[12] and $HoNi_2B_2C$.[13]

Despite over 50 years of research in the area of rare-earth transition-metal chalcogenides, the field remains relatively narrow. This is especially evident when one considers the drastic decrease in the number of ternary compounds as we move from the sulfides to the tellurides. For example, if we consider those compounds that have been characterized by single-crystal diffraction methods, then ternary 4f-sulfides are known for all 3d metals but far from all 4d or 5d metals, and only a few 3d/4f selenides and tellurides are known. Unfortunately, the situation is only slightly better for quaternary systems, although for such systems improved synthetic methods, especially the reactive-flux technique,[14] are bringing about a rapid increase in the number of new compounds.

II. Scope of This Review

This review is limited to compounds that have been characterized by single-crystal diffraction methods, although occasional reference is made to related compounds characterized by powder diffraction methods. In this way we reduce the number of compounds to be considered and those we do consider are subject to less uncertainty as to their stoichiometry and the relation of structure to physical properties. Even within those compounds characterized by diffraction methods we impose further restrictions: (1) we do not consider the large and growing area of "misfit structures"[15] of the "$LnMQ_3$" or $(LnQ)_xMQ_2$ compositions, (2) we do not consider oxychalcogenides, and (3) we do not consider doped or intercalation compounds, all subjects in their own right. We note in passing that there is a relatively recent review that is concerned with metal chalcogenides of Th and U.[16]

The various compounds reported within this review are sorted into the categories of ternary and quaternary compounds. In each category the materials are listed roughly in order of increasing structural complexity. A brief account of synthesis, structure, and physical properties is provided. Tables 1−4 offer lists of the individual compounds sorted by common structural features. These tables clearly depict the wide variation in structure type among the solid-state 3d/4f chalcogenides.

III. Ternary Compounds

The majority of ternary compounds discussed here have been synthesized by conventional high-temperature syntheses, although increasingly with the addition of alkali-metal halide fluxes, such as KCl or KI. Such fluxes enable lower reaction temperatures, shorter heating profiles, and improved crystal growth. In general, the thermodynamic products are obtained in these syntheses; Q−Q bonding is absent, and the compounds are "classic" in that oxidation states are readily assigned. However, some of the compounds discussed are "nonclassic" in that formal oxidation states cannot be assigned. This is especially true in some tellurides, where a range of Te−Te bond lengths occurs. Many of these nonclassic compounds have low-dimensional structures. They have generally been synthesized by the reactive-flux method[14] and may be kinetic products.

We generally choose chalcogenides as structure types in the descriptions below, even though some correspond to other known structure types, e.g., oxides.

A. $LnCuQ_2$ Phases

Compounds with this formula that have been characterized by single-crystal diffraction studies include $LaCuS_2$,[17] $SmCuS_2$,[18] $YCuS_2$,[19] LaCuSTe,[20] and SmCuSTe.[20]

1. Syntheses

$LaCuS_2$ was prepared by the reaction of La_2S_3 and Cu_2S at 1673 K under a current of H_2S. The high-temperature reaction of Sm_2S_3 and Cu_2S produced

Table 1. Summary of the Rare-Earth Transition-Metal Chalcogenide Three-Dimensional Phases

compound	structure type	related compounds	section	figure number
$CeCrSe_3$	$[NH_4][CdCl_3]$		III.I	11
Dy_6FeTe_2	Zr_6CoAl_2	$Er_7Ni_2Te_2$	III.F	8
$Er_{0.66}Cu_2S_2$	*anti*-La_2O_3		III.E	7
Er_2CdS_4	cubic spinel		III.K.1	13
Er_2CrS_4	Er_2CrS_4	Er_2MnS_4	III.K.4	15
Er_2MnS_4	Y_2MnS_4	Er_2CrS_4	III.K.3	
$Er_7Ni_2Te_2$	$Er_7Ni_2Te_2$	Dy_6FeTe_2	III.H	10
$Eu_{0.59}Nb_5Se_8$	$Eu_{0.59}Nb_5Se_8$		III.S	22
$Eu_6Cu_{12}Fe_{13}S_{27}$	$Ba_6Cu_{12}Fe_{13}S_{27}$		IV.S	42
$EuZrSe_3$	$[NH_4][CdCl_3]$		III.I	11
$Gd_{0.66}Cr_2S_4$	$Sm_{0.66}Cr_2S_4$		III.L	16
$Gd_{0.66}Cu_2S_2$	*anti*-La_2O_3		III.E	7
$GdAgS_2$	LnS		III.B	
$HoAgS_2$	LnS		III.B	
$K_{0.5}Ba_{0.5}DyCu_{1.5}Te_3$	$K_{0.5}Ba_{0.5}DyCu_{1.5}Te_3$	$KZrCuS_3$	IV.D	
$La_2Fe_{1.76}S_5$	$La_2Fe_{1.76}S_5$	$La_2Fe_2S_5$	III.N	
$La_2Fe_{1.87}S_5$	$La_2Fe_{1.87}S_5$	$La_2Fe_2S_5$	III.N	
$La_2Fe_2S_5$	$La_2Fe_2S_5$		III.N	18
La_3CuSiS_7	$Ce_6Al_{3.33}S_{14}$		IV.N	36
$LaPbCuS_3$	$LaPbCuS_3$	α-La_2S_3	IV.A	25
$Sm_{0.66}Cr_2S_4$	$Sm_{0.66}Cr_2S_4$		III.L	16
Tm_2ZnS_4	olivine		III.K.2	14
$YbAgS_2$	NaCl		III.B	

Table 2. Summary of the Rare-Earth Transition-Metal Chalcogenide Layered Phases

compound	structure type	related compounds	section	figure number
β-$BaLaCuSe_3$	Eu_2CuS_3		IV.C.2.b	12
$Ba_4Gd_2Cd_3S_{10}$	$Ba_4Nd_2Cd_3Se_{10}$		IV.P	38
$Ba_4Nd_2Cd_3Se_{10}$	$Ba_4Nd_2Cd_3Se_{10}$		IV.P	38
$Ba_4Sm_2Cd_3S_{10}$	$Ba_4Nd_2Cd_3Se_{10}$		IV.P	38
$Ba_4Tb_2Cd_3S_{10}$	$Ba_4Nd_2Cd_3Se_{10}$		IV.P	38
$BaDyCuTe_3$	$KZrCuS_3$		IV.C.2.a	26
$BaErCuS_3$	$KZrCuS_3$		IV.C.2.a	26
$BaGdAuSe_3$	$KZrCuS_3$		IV.C.2.a	26
$BaGdCuSe_3$	$KZrCuS_3$		IV.C.2.a	26
$BaLaCuTe_3$	Eu_2CuS_3		IV.C.2.b	12
$BaYAgSe_3$	$KZrCuS_3$		IV.C.2.a	26
$BaYAgTe_3$	$KZrCuS_3$		IV.C.2.a	26
$BaYCuTe_3$	$KZrCuS_3$		IV.C.2.a	26
$CsCe_2CuS_6$	KEu_2CuS_6		IV.L	34
$CsCeCuS_3$	$KZrCuS_3$		IV.B	26
$CsGdZnSe_3$	$KZrCuS_3$		IV.B	26
$Er_{4.6}Mn_{0.4}S_7$	Y_5S_7		III.P	20
$Er_6Cr_2S_{11}$	$Er_6Cr_2S_{11}$	$Yb_6Fe_2S_{11}$	III.T	23
$ErAgSe_2$	$ErAgSe_2$		III.B	4
Eu_2CuS_3	Eu_2CuS_3		III.J	12
$EuCu_{0.66}Te_2$	$CaMnBi_2$	$KEuCu_2Te_4$	III.C	
Gd_3CrSe_6	U_3ScS_6		III.O	19
$Gd_8CrTe_{13}Cl$	$Sm_8CrTe_{13}Cl$		IV.R	41
Ho_4FeS_7	Y_5S_7		III.P	20
$K_2CeCu_2S_4$	$K_2CeCu_2S_4$		IV.G	
KCe_2CuS_6	KEu_2CuS_6		IV.L	34
KCe_2CuSe_6	KEu_2CuS_6		IV.L	34
$KCeCuTe_4$	$KCeCuTe_4$		IV.E	29
KEu_2CuS_6	KEu_2CuS_6		IV.L	34
$KEuCu_2Te_4$	$CaMnBi_2$	$EuCu_{0.66}Te_2$	IV.H	5
La_4NiS_7	La_4NiS_7	K_2NiF_4	III.Q	
$LaCuS_2$	$LaCuS_2$		III.A	1
$LaCuSTe$	$LaCuSTe$	$LaCuS_2$	III.A	
$Rb_2CeCu_3Te_5$	$Rb_2CeCu_3Te_5$		IV.J	32
Sm_3CrSe_6	U_3ScS_6		III.O	19
$Sm_8CrTe_{13}Cl$	$Sm_8CrTe_{13}Cl$		IV.R	41
$SmCuS_2$	$LaCuS_2$		III.A	1
$SmCuSTe$	$SmCuSTe$	$LaCuS_2$	III.A	3
Tb_3CrSe_6	U_3ScS_6		III.O	19
$Tb_8CrTe_{13}Cl$	$Sm_8CrTe_{13}Cl$		IV.R	41
Y_2HfS_5	U_3S_5		III.M	17
Y_4FeS_7	Y_5S_7		III.P	20
$Y_5Fe_2Te_2$	$Y_5Fe_2Te_2$		III.G	9
$Yb_6Fe_2S_{11}$	$Yb_6Fe_2S_{11}$	$Er_6Cr_2S_{11}$	III.T	23
$YCuS_2$	$YCuS_2$	$LaCuS_2$	III.A	2

Table 3. Summary of the Rare-Earth Transition-Metal Chalcogenide Cluster and Linear Chain Phases

compound	structure type	structural features	related compounds	section	figure number
$DyCu_{0.32}Te_2$	$LaCu_{0.28}Te_2$	Te chains		III.D	6
$Eu_2Re_6S_{11}$	$Eu_2Re_6S_{11}$	cluster		III.U	24
$Gd_3Cu_2Te_7$	$Gd_3Cu_2Te_7$	Te chains		III.R	21
$GdCu_{0.33}Te_2$	$LaCu_{0.28}Te_2$	Te chains		III.D	6
$La_{15.9}Cr_{5.4}S_{32}$	$La_{15.9}Cr_{5.4}S_{32}$	cluster	$La_{3.266}M_{1.1}S_6$	III.V	
$La_{3.266}Fe_{1.1}S_6$	$La_{3.266}Mn_{1.1}S_6$	cluster	$La_{15.9}Cr_{5.4}S_{32}$	III.V	
$La_{3.266}Mn_{1.1}S_6$	$La_{3.266}Mn_{1.1}S_6$	cluster	$La_{15.9}Cr_{5.4}S_{32}$	III.V	
$LaCu_{0.28}Te_2$	$LaCu_{0.28}Te_2$	Te chains		III.D	6
$LaCu_{0.40}Te_2$	$LaCu_{0.28}Te_2$	Te chains		III.D	6
$NdCu_{0.37}Te_2$	$LaCu_{0.28}Te_2$	Te chains		III.D	6
$SmCu_{0.34}Te_2$	$LaCu_{0.28}Te_2$	Te chains		III.D	6

Table 4. Summary of the Rare-Earth Transition-Metal Chalcogenide Tunnel Phases

compound	structure type	related compounds	section	figure number
α-$BaLaCuSe_3$	$BaLaCuS_3$	$BaErAgS_3$	IV.C.2.c	27
$Ba_2LaAg_5S_6$	$Ba_2LaAg_5S_6$		IV.M	35
$Ba_2YAg_5S_6$	$Ba_2LaAg_5S_6$		IV.M	35
$BaErAgS_3$	$BaErAgS_3$	$BaLaCuS_3$	IV.C.2.d	28
$BaLaCuS_3$	$BaLaCuS_3$	$BaErAgS_3$	IV.C.2.c	27
$Cs_3Gd_4Cu_5Te_{10}$	$Rb_3Nd_4Cu_5Te_{10}$		IV.Q	39, 40
$CsGd_2Ag_3Se_5$	$RbSm_2Ag_3Se_5$	ALn_2MQ_4, $Rb_2Gd_4Cu_4S_9$	IV.K	33
$CsLa_2CuSe_4$	KGd_2CuS_4	$ALn_2M_3Q_5$, $Rb_2Gd_4Cu_4S_9$	IV.F	30
$CsSm_2CuSe_4$	KGd_2CuS_4	$ALn_2M_3Q_5$, $Rb_2Gd_4Cu_4S_9$	IV.F	30
$CsTb_2Ag_3Se_5$	$RbSm_2Ag_3Se_5$	ALn_2MQ_4, $Rb_2Gd_4Cu_4S_9$	IV.K	33
$K_2CeAg_3Te_4$	$K_2CeAg_3Te_4$		IV.I	31
$K_3Dy_4Cu_5Te_{10}$	$K_3Dy_4Cu_5Te_{10}$		IV.Q	39, 40
$K_3Er_4Cu_5Te_{10}$	$K_3Sm_4Cu_5Te_{10}$		IV.Q	39, 40
$K_3Gd_4Cu_5Te_{10}$	$K_3Sm_4Cu_5Te_{10}$		IV.Q	39, 40
$K_3Sm_4Cu_5Te_{10}$	$K_3Sm_4Cu_5Te_{10}$		IV.Q	39, 40
KGd_2CuS_4	KGd_2CuS_4	$ALn_2M_3Q_5$, $Rb_2Gd_4Cu_4S_9$	IV.F	30
$Rb_2Gd_4Cu_4S_9$	$Rb_2Gd_4Cu_4S_9$	ALn_2MQ_4, $ALn_2M_3Q_5$	IV.O	37
$Rb_3Dy_4Cu_5Se_{10}$	$Rb_3Gd_4Cu_5Se_{10}$		IV.Q	39, 40
$Rb_3Gd_4Cu_5Se_{10}$	$Rb_3Gd_4Cu_5Se_{10}$		IV.Q	39, 40
$Rb_3Gd_4Cu_5Te_{10}$	$Rb_3Nd_4Cu_5Te_{10}$		IV.Q	39, 40
$Rb_3Nd_4Cu_5Te_{10}$	$Rb_3Nd_4Cu_5Te_{10}$		IV.Q	39, 40
$RbDy_2CuSe_4$	KGd_2CuS_4	$ALn_2M_3Q_5$, $Rb_2Gd_4Cu_4S_9$	IV.F	30
$RbEr_2Cu_3S_5$	$RbSm_2Ag_3Se_5$	ALn_2MQ_4, $Rb_2Gd_4Cu_4S_9$	IV.K	33
$RbGd_2CuSe_4$	KGd_2CuS_4	$ALn_2M_3Q_5$, $Rb_2Gd_4Cu_4S_9$	IV.F	30
$RbNd_2CuS_4$	KGd_2CuS_4	$ALn_2M_3Q_5$, $Rb_2Gd_4Cu_4S_9$	IV.F	30
$RbSm_2Ag_3Se_5$	$RbSm_2Ag_3Se_5$	ALn_2MQ_4, $Rb_2Gd_4Cu_4S_9$	IV.K	33
$RbSm_2CuS_4$	KGd_2CuS_4	$ALn_2M_3Q_5$, $Rb_2Gd_4Cu_4S_9$	IV.F	30
$RbSm_2CuSe_4$	KGd_2CuS_4	$ALn_2M_3Q_5$, $Rb_2Gd_4Cu_4S_9$	IV.F	30

$SmCuS_2$. $YCuS_2$ was prepared from a mixture of Y, Cu, and S at 1173 K. LnCuSTe (Ln = La, Sm) was formed from the reaction of Ln, Cu, S, and Te at 1123 K in a KI flux.

2. Structures

The structures of $LaCuS_2$ (Figure 1), $YCuS_2$ (Figure 2), LaCuSTe, and SmCuSTe (Figure 3) are similar. Each may be thought of as consisting of CuS_2 or

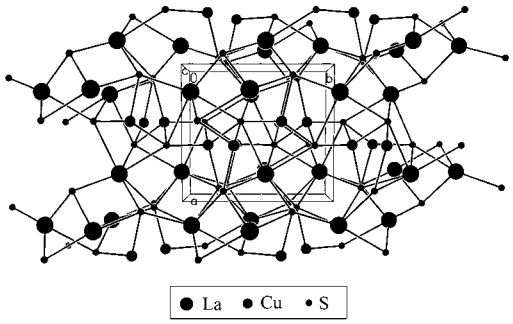

Figure 1. $LaCuS_2$ structure type. Unless otherwise noted, in this and succeeding figures large black spheres represent Ln, intermediate-size black spheres represent M, and small black spheres represent Q atoms. The unit cell is outlined here and in most succeeding figures.

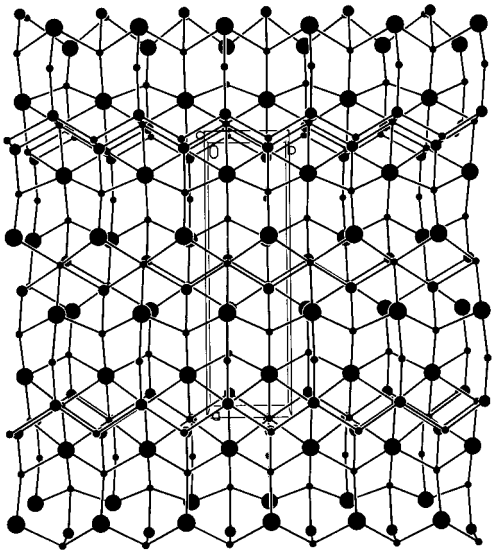

Figure 2. $YCuS_2$ structure.

CuSTe layers stacked perpendicular to the *a* axis and separated by Ln atoms. The coordination environment of the Ln atoms varies and is octahedral ($YCuS_2$), monocapped trigonal prismatic ($LaCuS_2$ and

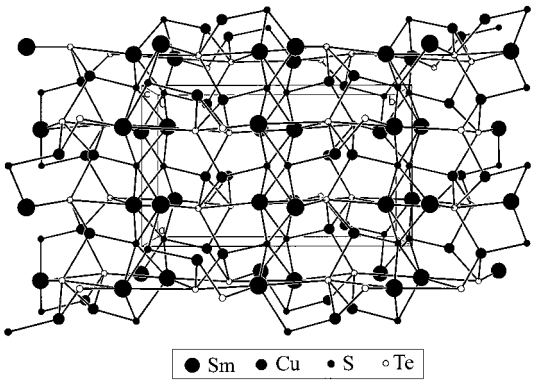

Figure 3. SmCuSTe structure. The small open spheres represent Te atoms.

SmCuSTe), or bicapped trigonal prismatic (LaCuSTe). The compound $SmCuS_2$ is isostructural with $LaCuS_2$.

3. Physical Properties[21]

Electrical resistivity, thermopower, and magnetic susceptibility measurements were made for $LnCuS_2$ (Ln = La, Nd, Sm, Gd, Dy, Ho, Yb, Lu, Y). These compounds are p-type semiconductors with wide band gaps; they exhibit no long-range magnetic order.

4. Theoretical Considerations[20]

Band structure calculations for LnCuSTe (Ln = La, Sm) indicate that these compounds should be semiconductors with smaller band gaps than that in $LaCuS_2$.

B. $LnAgQ_2$ Phases

These compounds include $LnAgS_2$ (Ln = Sm, Gd−Yb, Y),[22] $LnAgSe_2$ (all Ln except Pm and Eu),[23−27] and $LnAgTe_2$ (Ln = Gd, Dy−Er, Y).[28]

1. Syntheses

$ErAgSe_2$ was prepared by the reaction of Er, Ag, and Se at 1473 K. Microcrystalline powders of $LnAgS_2$ (Ln = Gd, Ho, Yb) were prepared from the combination of the elements at 1100 K or from a mixture of Ln_2S_3 and Ag at 1100 K under H_2S gas. Single crystals of $LnAgS_2$ (Ln = Gd, Ho, Yb) were obtained with the use of $[NH_4]_2[PbCl_6]$ as a chemical transport agent in the temperature gradient 1100−1300 K. The remaining sulfides and selenides were prepared by heating mixtures of Ln_2Q_3 and Ag_2Q at temperatures greater than 873 K, whereas the tellurides were obtained from the reactions of the elements at 1373 K.

2. Structures

Only $ErAgSe_2$[26] and $LnAgS_2$ (Ln = Gd, Ho, Yb)[27] have been studied by single-crystal X-ray diffraction methods.

$ErAgSe_2$ is a layered structure (Figure 4). The Er atom has octahedral coordination, and the Ag atom has tetrahedral coordination. The $AgSe_4$ tetrahedra form open chains along the *c* axis and create channels in which the Ag cations may move. These chains of

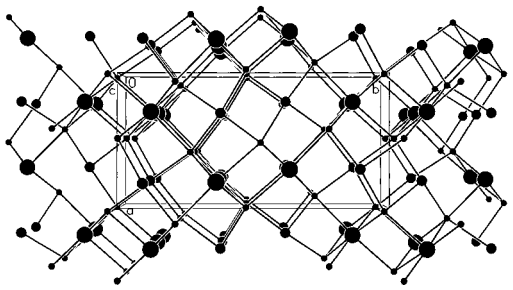

Figure 4. View of the structure of $ErAgSe_2$ along the *c* axis.

$AgSe_4$ tetrahedra connect with the $ErSe_6$ octahedra to form layers that stack along the *a* axis.

The structure of the $LnAgS_2$ (Ln = Gd, Ho) compounds was solved from a limited data set. The three-dimensional structure is a superstructure of the LnS (NaCl) type with one-half of the Ln cations replaced with Ag. The Ag atom is in a severely distorted octahedral environment with two short, three intermediate, and one long Ag−S bond. The Ln atom is octahedrally coordinated.

$YbAgS_2$ adopts the NaCl structure type with Ag and Yb randomly distributed over the cation sites. The cations are octahedrally coordinated.

3. Physical Properties

a. Electrical Conductivity.[26] $ErAgSe_2$ is an ionic conductor ($\sigma_{298} = 6.5 \times 10^{-4}$ and $\sigma_{673} = 1.5 \times 10^{-1}$ ohm^{-1} cm^{-1}).

b. Magnetic Properties.[27] $GdAgS_2$ is paramagnetic over the temperature range 4.2−300 K. The μ_{eff} value derived from the magnetic data corresponds to Gd^{III}.

4. Related Compounds[27]

From unit cell parameters obtained from single crystals, the structure of $ErAgS_2$ appears to be related to that of the $LnAgS_2$ (Ln = Gd, Ho) compounds.

C. $EuCu_{0.66}Te_2$[29]

1. Synthesis

This material was synthesized at 1123 K from a reactive flux of Rb_2Te/Te containing Cu and Eu.

2. Structure

$EuCu_{0.66}Te_2$ exhibits a layered structure that is closely related to that of $KEuCu_2Te_4$ (Figure 5). If the occupancy of the Cu site in $KEuCu_2Te_4$ is reduced to two-thirds and if K is replaced with Eu, then the $EuCu_{0.66}Te_2$ structure is obtained.

D. $LnCu_xTe_2$[30,31]

1. Syntheses

$LaCu_{0.28}Te_2$[30] was prepared from the elements in the presence of I_2 at 1275 K. $LaCu_{0.40}Te_2$, $NdCu_{0.37}Te_2$, $SmCu_{0.34}Te_2$, $GdCu_{0.33}Te_2$, and $DyCu_{0.32}Te_2$[31] were prepared from the elements at 1073 K with the use of the corresponding $LnCl_3$ as flux.

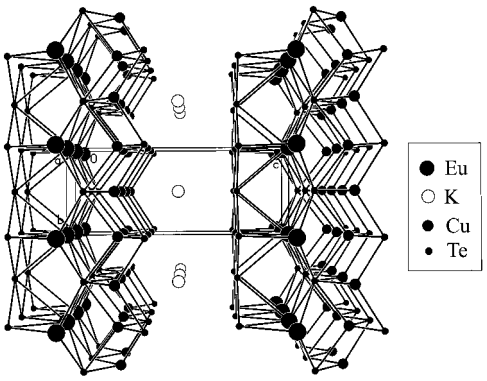

Figure 5. $KEuCu_2Te_4$ structure. Unless otherwise noted, in this and succeeding figures the unfilled spheres represent the A atoms.

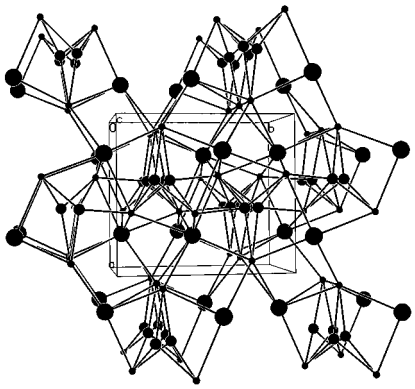

Figure 6. $LnCu_xTe_2$ structure, as typified by the structure of $LaCu_{0.40}Te_2$.

2. Structure

In this structure (Figure 6) the Ln atoms are eight coordinate in a bicapped trigonal-prismatic arrangement and the Cu atoms are tetrahedrally coordinated. These polyhedra share edges to create pentagonal tunnels along the *c* axis. The Cu atoms partially occupy sites within the tunnels to form zigzag chains parallel to the *c* axis. An important feature of this structure type is the infinite linear Te−Te chain running parallel to *c*, with Te−Te distances decreasing from 3.1558(5) Å in $LaCu_{0.40}Te_2$ to 3.0273(3) Å in $DyCu_{0.32}Te_2$.

3. Physical Properties[31]

a. Magnetic Properties. $GdCu_{0.33}Te_2$ is paramagnetic above 7 K; the μ_{eff} value derived from the magnetic data corresponds to Gd^{III}.

b. Transport Properties. Conductivity measurements indicate that these compounds semiconduct in the *c* direction.

Thermopower data exhibit p-type behavior for all materials. $NdCu_{0.37}Te_2$, $SmCu_{0.34}Te_2$, and $GdCu_{0.33}Te_2$ show similar behavior as the temperature decreases from 300 K where the values are on the order of 200−400 μV/K. The magnitude of the thermopower increases as the temperature decreases, which is characteristic of a semiconductor material. However, the thermopower data for the three compounds exhibit very high peaks of approximately 900 μV/K in the vicinity of 150 K, followed by a rapid decrease at lower temperatures. Although this behavior is more typical of metallic materials, this magnitude of the thermopower is usually associated with semiconductor behavior. $LaCu_{0.40}Te_2$ shows considerably lower thermopower values, with a linear decrease with temperature.

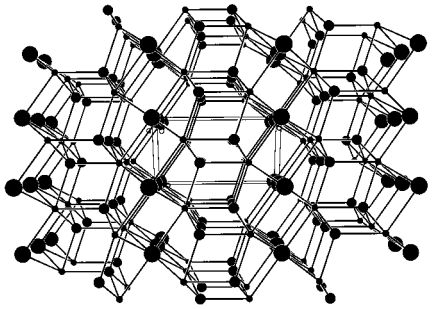

Figure 7. $Ln_{0.66}Cu_2S_2$ structure, as represented by that of $Gd_{0.66}Cu_2S_2$. In the structure Ln atoms occupy two-thirds of the octahedral sites; these are shown fully occupied here.

4. Theoretical Considerations[31]

Extended Hückel calculations on $LaCu_xTe_2$ ($x = {}^1/_3$, ${}^1/_2$, 1) provide some insight into these physical properties.

5. Related Compounds

The compounds $LnCu_{0.5}Te_2$ (Ln = La−Nd, Sm)[32,33] and $LnCu_{0.5}Te_{1.75}$ (La = La, Nd)[32] have been prepared, and their unit cells have been determined from powder diffraction data.

E. $Ln_{0.66}Cu_2S_2$ (Ln = Gd,[34] Er[35])

1. Syntheses

$Gd_{0.66}Cu_2S_2$ was prepared from a mixture of Cu_2S, Gd, and S at 1073−1173 K with I_2 as a transport agent. $Er_{0.66}Cu_2S_2$ was synthesized from Cu_2S and Er_2S_3 at 1473 K under a flow of H_2S.

2. Structure

These compounds exhibit an uncharacterized superstructure. The average substructure (Figure 7), obtained from limited data sets, is of the *anti*-La_2O_3 structure type. This three-dimensional structure consists of hexagonal closest packing of S atoms with the Ln atoms occupying two-thirds of the octahedral sites and the Cu atoms occupying the tetrahedral sites. The octahedral vacancies exhibit intralayer order and interlayer short-range order.

F. Dy_6FeTe_2[36]

1. Synthesis

This compound and the related Ln_6MTe_2 compounds were synthesized from the stoichiometric reactions of Ln, $LnTe_2$, and M at 1373 K.

2. Structure

The structure (Figure 8), which is of the Zr_6CoAl_2 or Zr_6FeSn_2 type,[37] contains two independent Dy atoms. It is constructed from face-shared trigonal prisms of Dy1 (inner) atoms centered by Fe atoms with each rectangular face of the prism capped by a

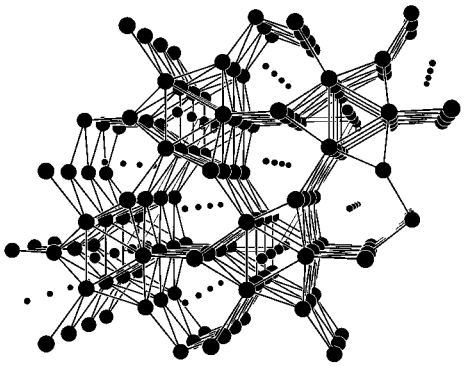

Figure 8. Structure of Dy_6FeTe_2 viewed down the *c* axis. The Dy−Te bonds have been removed for clarity.

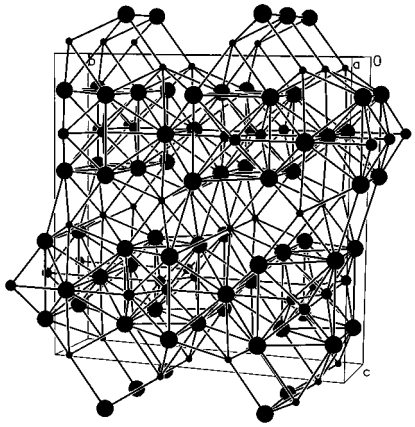

Figure 9. Structure of $Y_5Fe_2Te_2$.

Dy2 (outer) atom. This arrangement yields tricapped trigonal prisms of Dy atoms that are centered by Fe atoms. The prisms are interconnected through shared basal Dy1 faces along the *c* axis to form infinite chains. The tricapped trigonal prisms are interconnected along the *a* and *b* axes by means of Dy1−Dy2 interchain bonds to form the overall three-dimensional structure. The Te atoms reside in the channels between the prisms.

3. Theoretical Considerations

Extended Hückel band calculations provide some insight into the nature of the structure; these calculations imply metallic character for the compound.

4. Related Compounds[36]

On the basis of powder X-ray data the compounds Dy_6MTe_2 (M = Co, Ni) and Dy_6MTe_2 (Ln = La, Y) are isostructural with Dy_6FeTe_2.

G. $Y_5Fe_2Te_2$[38]

1. Synthesis

This compound and $Y_5M_2Te_2$ (M = Co, Ni) were synthesized by the reactions of Y_2Te_3, Y, and M at 1323 K.

2. Structure

The structure of $Y_5Fe_2Te_2$ is composed of infinite heterometallic layers that run parallel to the *b* axis (Figure 9). The Y atoms form body-centered cubes and puckered six-membered rings that sandwich two types of Fe atoms. The Fe atoms are coordinated in a trigonal-prismatic arrangement to six Y atoms. These trigonal prisms share rectangular faces to form zigzag chains of Fe atoms. The intermetallic layers are separated by Te atoms.

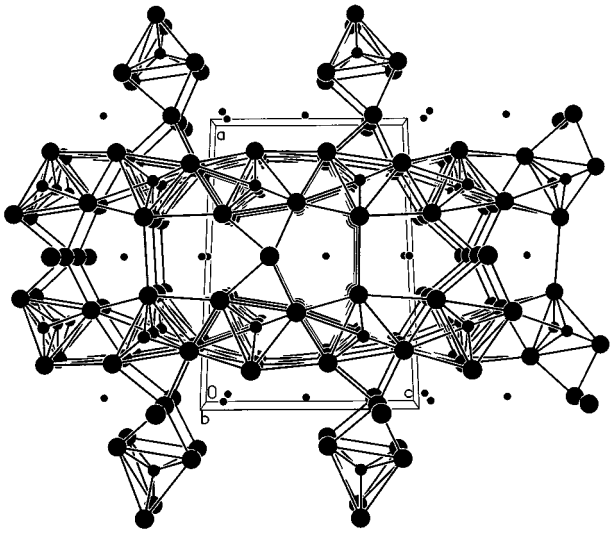

Figure 10. Structure of $Er_7Ni_2Te_2$. All Er−Te bonds have been removed.

3. Related Compounds

$Y_5M_2Te_2$ (M = Co, Ni)[38] are isostructural with M = Fe, on the basis of X-ray powder data.

H. $Er_7Ni_2Te_2$[39]

1. Synthesis

The compound was synthesized by the reaction of Er, Er_3Ni, and $NiTe_2$ at 1373 K.

2. Structure

This structure (Figure 10) is similar to that of Dy_6FeTe_2 (Figure 8). The basic structural motif of $Er_7Ni_2Te_2$ is the Ni-centered tricapped trigonal prism of Er atoms. The structures are also similar in that the prisms share their triangular bases to form infinite chains that propagate along the *b* axis. These infinite chains are condensed to form corrugated layers with the capping Er atom of one prism being an inner Er atom on an adjacent prism. Finally, vertex-sharing between layers results in the overall three-dimensional structure.

3. Magnetic Properties

$Er_7Ni_2Te_2$ is paramagnetic, but it exhibits an ordering transition at 16.5 K that is ascribed to an indirect exchange interaction among Er moments. It is the first metal-rich rare-earth chalcogenide for which a magnetic transition has been observed.

4. Theoretical Considerations

Results from extended Hückel calculations are consistent with metallic behavior.

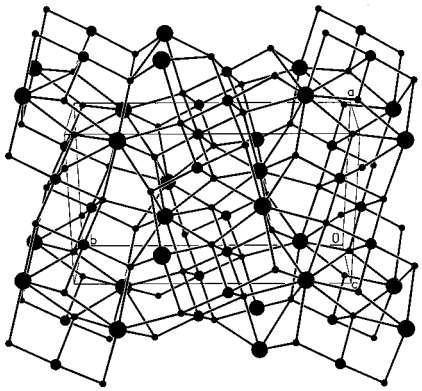

Figure 11. Structure of $CeCrSe_3$.

I. $LnMSe_3$ Phases

1. Syntheses

Some of these compounds were synthesized from mixtures of Ln_2Se_3 and M_2Se_3 at 1273 K. The other materials were formed from the reactions of the constituent elements at 1073 or 1273 K.

2. Structures

Many of these compounds belong to the $[NH_4][CdCl_3]$ structure type,[40] a class of ABX_3 compounds that are primarily differentiated by the coordination number of the large A cation. This coordination number may vary from three to nine. These compounds include $LnCrSe_3$ (Ln = La−Nd),[41] $LnCrSe_3$ (Ln = Tb, Dy),[42] and $EuZrSe_3$.[43] However, only $CeCrSe_3$[41] and $EuZrSe_3$ were studied by single-crystal diffraction methods.

The three-dimensional structure of $CeCrSe_3$ (Figure 11) comprises $CrSe_6$ octahedra and $CeSe_9$ tricapped trigonal prisms. The $CrSe_6$ octahedra share edges to form a continuous double chain along the *c* axis. These double chains are linked together by the $CeSe_9$ prisms.

The structure of $EuZrSe_3$ differs only slightly from that of $CeCrSe_3$. It contains $EuSe_8$ bicapped trigonal prisms.

3. Physical Properties

a. Magnetic Properties.[44,45] The magnetic properties of these compounds are relatively complicated. Each $LnCrSe_3$ (Ln = La−Nd) compound exhibits an antiferromagnetic transition between 160 K ($LaCrSe_3$) and 190 K ($NdCrSe_3$). However, above the Néel temperature there are some ferromagnetic interchain interactions, whereas at low temperatures there may be some weak ferromagnetic interactions resulting from the canting of spins. The complex magnetic behavior is ascribed to the Cr^{III} cations, and it is assumed that there are no interactions between these cations and the Ln^{III} cations.

b. Other Properties. The densities, electrical conductivities, thermopowers, and microhardness of the compounds $LnCrSe_3$ (Ln = Tb, Dy)[42] have been determined on polycrystalline samples and pressed pellets. These compounds are p-type semiconductors. Additionally, resistivity measurements on single crystals of the $LnCrSe_3$ (Ln = La−Pr) compounds[45] indicate semiconducting behavior.

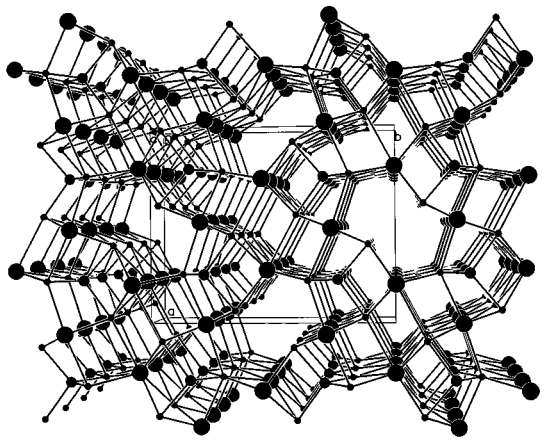

Figure 12. Structure of Eu_2CuS_3.

J. Eu_2CuS_3[46]

1. Synthesis

The material was prepared from a stoichiometric mixture of EuS and Cu_2S under a flow of H_2S at 973−1073 K.

2. Structure

Eu exists in the +II and +III oxidation states in this compound. The structure (Figure 12) consists of $Eu^{III}S_6$ octahedra, $Eu^{II}S_7$ monocapped trigonal prisms, and CuS_4 tetrahedra. The tetrahedra form chains parallel to the *c* axis. These chains participate in vertex-sharing with the EuS_6 octahedra to form $^2_\infty[EuCuS_3^{2-}]$ layers that stack perpendicular to the *b* axis. The $^2_\infty[EuCuS_3^{2-}]$ layers are separated by a layer of EuS_7 trigonal prisms.

3. Related Structures

β-$BaLaCuSe_3$[47] and $BaLaCuTe_3$[48] are of this structure type, with La^{III} in place of Eu^{III}, Ba^{II} in place of Eu^{II}, and Se or Te in place of S.

K. Ln_2MQ_4 Phases

The Ln_2MQ_4 phases are the most extensively characterized rare-earth transition-metal chalcogenides. These compounds adopt several different three-dimensional structure types, including the cubic spinel and olivine structures. Here, selected compounds have been chosen to represent these structure types.

1. Er_2CdS_4[49]

Although Er_2CdS_4 is chosen to represent the cubic spinel phases, there have been several other single-crystal diffraction studies completed on this interesting family of compounds. These studies include Ln_2CdS_4 (Ln = Tm, Yb,[50] Y[51]), Ln_2FeS_4 (Ln = Yb, Lu),[52,53] and Ln_2CdSe_4 (Ln = Ho, Tm).[54]

a. Synthesis. Er_2CdS_4 was obtained from the reaction of CdS and Er_2S_3 at 1273 K with KBr as flux.

b. Structure. This compound adopts the cubic spinel structure (Figure 13). It consists of cubic

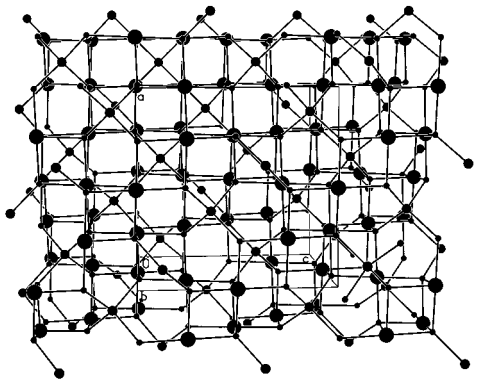

Figure 13. Cubic spinel structure, as represented by that of Er_2CdS_4.

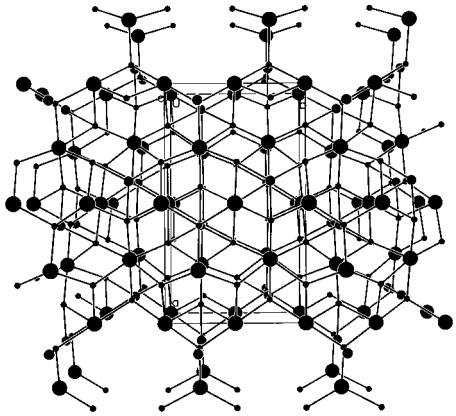

Figure 14. Olivine structure type, as represented by that of Tm_2ZnS_4.

closest-packing of S atoms with Ln atoms in the octahedral interstices and M atoms in the tetrahedral ones.

c. Magnetic Properties. Magnetic susceptibility measurements indicate that the following compounds are paramagnetic: Ln_2MnQ_4 (Ln = Yb, Lu; Q = S, Se),[55−58] $Yb_2(MnMg)S_4$,[59] Yb_2FeS_4,[56−58] and Ho_2CdSe_4.[60] However, deviations from Curie−Weiss behavior were observed at low temperatures for Tm_2CdSe_4.[61] These are ascribed to crystal-field effects on the Ln ions. The compounds Er_2CdQ_4 (Q = S, Se)[60] and Lu_2FeS_4[58] undergo ferromagnetic and antiferromagnetic transitions, respectively.

d. Other Properties. The melting points, microhardness, densities, and optical properties of the Ln_2CdS_4 (Ln = Dy−Lu)[62−64] semiconductors have been measured. Thermopower measurements on Ln_2CdS_4 (Ln = Er, Yb)[63] show that electrons are the predominant carriers in these materials. Also, melting points, microhardness, and densities were obtained for Ln_2CdSe_4 (Ln = Dy, Ho).[64]

2. Tm_2ZnS_4[65]

a. Synthesis. The material was prepared from a mixture of ZnS and Tm_2S_3 at 1120 K with KBr as flux.

b. Structure. Tm_2ZnS_4 (Figure 14) adopts the olivine structure type.[66] It consists of hexagonal closest packing of S atoms with Tm atoms in the octahedral interstices and Zn atoms in the tetrahedral ones.

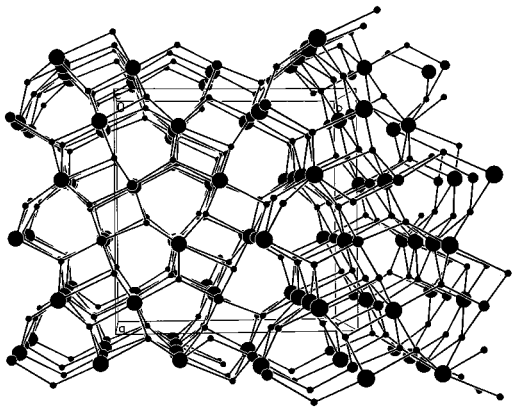

Figure 15. Structure of Er_2CrS_4 viewed along the *c* axis.

c. Related Compounds. Ln_2ZnS_4 (Ln = Er, Yb, Lu)[67] appear to be isostructural with Tm_2ZnS_4, based upon powder diffraction results.

d. Optical Properties. The Ln_2ZnS_4 (Ln = Dy, Ho, Tm, Lu, Y)[62,68] compounds are semiconductors with wide band gaps.

3. Er_2MnS_4[69]

a. Synthesis. The synthesis of Er_2MnS_4 was not reported.

b. Structure. This structure type is also frequently referred to as the Y_2MnS_4-type structure. Unfortunately, the atomic coordinates are unavailable, so we paraphrase the description of the structure.[69] The cell is orthorhombic and the metal atoms adopt two different coordination environments. One kind of Er atom is seven coordinate (7-octahedron); the second is octahedral and disordered with the Mn atom. The structure of this compound is supposedly similar to that of Er_2CrS_4 (Figure 15).

c. Related Compounds. X-ray powder diffraction results indicate that the compounds Ln_2MnS_4 (Ln = Tb−Tm, Y),[70] Ln_2FeS_4 (Ln = Ho−Tm),[70] and $Tb_2(MnMg)S_4$[71] belong to this structural family.

d. Magnetic Properties.[72] Magnetic susceptibility measurements were performed on polycrystalline samples of Er_2MnS_4 and Y_2MnS_4 down to 4.2 K. The compounds are paramagnetic and obey the Curie−Weiss law. There are no magnetic interactions between the Mn and Er cations in Er_2MnS_4, but there are strong short-range antiferromagnetic interactions among the Mn cations in Y_2MnS_4.

4. Er_2CrS_4[73]

a. Synthesis. Er_2CrS_4 was prepared from the reaction of Cr_2S_3 and Er_2S_3 at 2123 K.

b. Structure. In the structure of Er_2CrS_4 (Figure 15) there are ErS_6 octahedra and ErS_7 monocapped trigonal prisms. The Cr atoms occupy severely distorted octahedral sites with two long Cr−S interactions, thereby making them only four coordinate. This distortion, which results from the Jahn−Teller effect, prevents Er and Cr from disordering. In this structure the ErS_7 polyhedra form chains along the *c* axis. These chains share corners with chains of alternating ErS_6 octahedra and CrS_4 tetrahedra to form the overall three-dimensional structure.

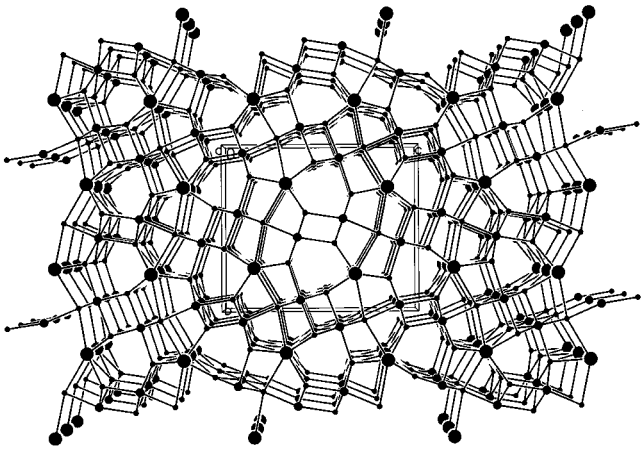

Figure 16. Subcell of the $Ln_{0.66}Cr_2S_4$ structure, as represented by $Sm_{0.66}Cr_2S_4$. In the structure Ln atoms occupy two-thirds of the prismatic sites; these are shown fully occupied here.

c. Related Compounds.[74] From X-ray powder studies the Ln_2CrS_4 (Ln = Ho−Yb, Y) compounds appear to possess this structure.

L. $Ln_{0.66}Cr_2S_4$ (Ln = Sm,[75] Gd[76])

1. Syntheses

$Sm_{0.66}Cr_2S_4$ and $Gd_{0.66}Cr_2S_4$ were prepared by the reaction of $LnCrO_3$ and Cr_2O_3 at 1573 K under H_2S gas flow.

2. Structure

The compounds adopt three-dimensional structures that are very similar (Figure 16). Both $Sm_{0.66}Cr_2S_4$ and $Gd_{0.66}Cr_2S_4$ exhibit a supercell and subcell for which the structures were solved. These compounds consist of staggered double chains of CrS_6 octahedra that share edges along the *a* axis. Ln-centered bicapped trigonal prisms connect these double chains of octahedra.

3. Related Compounds[77]

The unit cell parameters of $LnCr_3S_6$ (Ln = Gd, Dy, Ho, Er, Y), determined from powder diffraction data, are similar to those of the supercell of the $Ln_{0.66}Cr_2S_4$ compounds.

4. Magnetic Properties[76]

Magnetic measurements performed on single crystals of $Gd_{0.66}Cr_2S_4$ indicate that the material is paramagnetic over the temperature range 2−300 K.

M. Y_2HfS_5[78,79]

1. Synthesis

The compound was prepared at 1373 K from the reaction of Y, Hf, and S in the presence of I_2.

2. Structure

The structure of Y_2HfS_5 (Figure 17) is of the U_3Se_5 structure type[80] with the Y and Hf atoms substituting for U atoms in an ordered fashion. The Y atoms are coordinated to eight S atoms in a bicapped trigonal-prismatic arrangement. Eight-fold coordination of Y by S is rare; coordination numbers this high are usually found for the light rare-earth elements. The Hf atoms bond to seven S atoms in a monocapped trigonal-prismatic arrangement. These HfS_7 prisms participate in edge-sharing to form infinite chains parallel to the *b* axis. The chains form layers that stack perpendicular to the *a* axis and are separated by layers of YS_8 polyhedra.

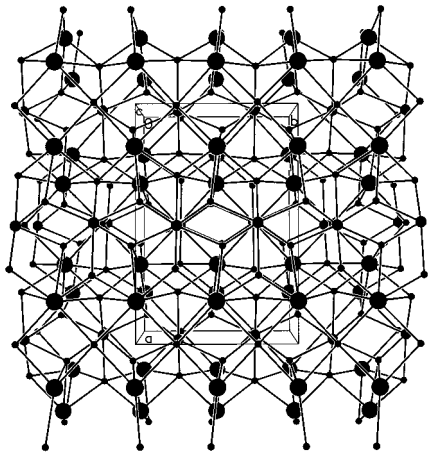

Figure 17. Structure of Y_2HfS_5.

3. Related Compounds[79]

The compounds Ln_2ZrS_5 (Ln = La, Sm, Gd, Ho, Er, Y), Ln_2HfS_5 (Ln = La, Ce, Sm, Gd, Ho, Er, Y), Ln_2ZrSe_5 (Ln = La, Sm, Gd, Tb), and Ln_2HfSe_5 (Ln = La, Ce) have been synthesized in an analogous manner and their lattice constants determined from powder diffraction data.

4. Physical Properties[79]

La_2ZrS_5 and Ce_2HfS_5 are high-resistivity semiconductors, whereas Sm_2HfS_5 shows lower resistivity, which is ascribed to the presence of an electronically active dopant, probably Sm^{II}.

N. $La_2Fe_2S_5$ Phases

1. Syntheses

$La_2Fe_2S_5$[69,81] was prepared from the reaction of La_2S_3 and FeS at 1223 K. The related compounds $La_2Fe_{1.87}S_5$[81] and $La_2Fe_{1.76}S_5$[82] were also synthesized at 1223 K from mixtures of La_2S_3 and $Fe_{0.95}S$ or $Fe_{0.83}S$, respectively.

2. Structures

The three-dimensional structure of $La_2Fe_2S_5$ (Figure 18) consists of two distinct La and Fe environments: a LaS_7 monocapped trigonal prism, a LaS_8 bicapped trigonal prism, an FeS_4 tetrahedron, and an FeS_6 octahedron. The Fe polyhedra share common edges. This edge-sharing produces chains, parallel to the *a* axis, formed by alternating Fe polyhedra. Four chains traverse each cell and are connected by the La-centered polyhedra.

The structures of $La_2Fe_{1.87}S_5$ and $La_2Fe_{1.76}S_5$ are derived from $La_2Fe_2S_5$. In both compounds vacancies are introduced on the Fe sites. These vacancies cause

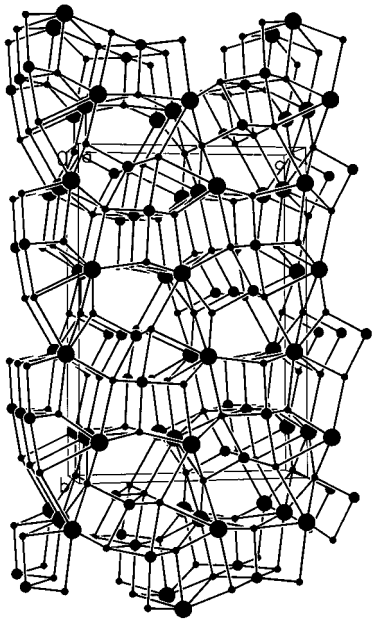

Figure 18. Structure of $La_2Fe_2S_5$ viewed down the *a* axis.

the Fe-centered chains to become staggered and the four-coordinate Fe centers to become five-coordinate.

3. Magnetic Properties

$La_2Fe_2S_5$ was originally reported to be an antiferromagnet with a Néel temperature of 11 K and a μ_{eff} value that corresponded to Fe^{II}.[83] However, neutron powder diffraction studies indicate an antiferromagnetic transition at 88 K.[84,85] The reason for this discrepancy is unknown. The neutron diffraction measurements also revealed superexchange interactions between Fe cations located in the chains.

4. Related Compounds

Neutron powder diffraction studies of La_2MnZnS_5[86] and La_2MnFeS_5[87] indicate that these compounds are isostructural with $La_2Fe_2S_5$.

O. Ln_3CrSe_6 (Ln = Gd,[88,89] Sm,[89] Tb[89])

1. Syntheses

These materials may be prepared from the stoichiometric reactions of the elements in a KBr flux at 1123 K.[89] Gd_3CrSe_6 may also be obtained from the thermal decomposition of $GdCrSe_3$ at 1073 K.[88]

2. Structure

The Ln_3CrSe_6 materials crystallize (Figure 19) in the U_3ScS_6[90] structure type. The structure consists of $LnSe_7$ octahedra (7-octahedron), $LnSe_8$ bicapped trigonal prisms, and $CrSe_6$ octahedra. The Ln-centered polyhedra share edges and vertices in the *a* direction to form a triple layer. In the *b* direction the Ln triple layers are separated by a single layer of $CrSe_6$ octahedra. The layers are connected by edge-sharing and corner-sharing of $CrSe_6$ octahedra and Ln-centered polyhedra.

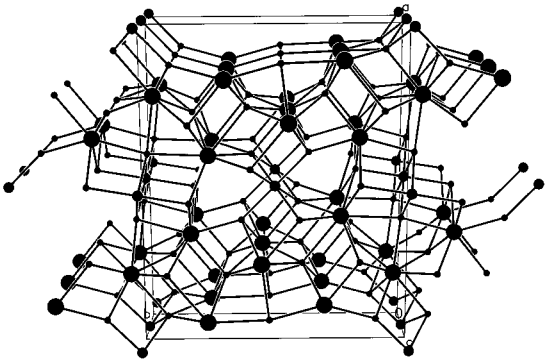

Figure 19. U_3ScS_6 structure type adopted by the Ln_3CrSe_6 compounds.

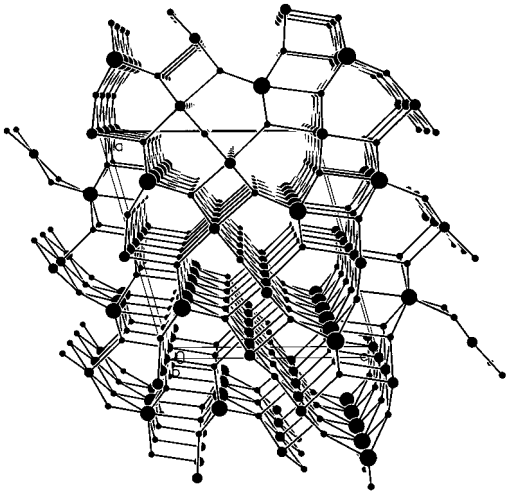

Figure 20. View of the structure of Ho_4FeS_7 along the *b* axis. The cation sites represented by the intermediate-size spheres are statistically occupied by Ho and Fe in a 3:1 ratio.

3. Physical Properties

a. Magnetic Properties.[89] Sm_3CrSe_6 and Tb_3CrSe_6 are paramagnetic down to 5 K. Gd_3CrSe_6 exhibits an antiferromagnetic transition at 10 K. Since Sm_3CrSe_6 and Tb_3CrSe_6 do not order magnetically, the antiferromagnetic transition of Gd_3CrSe_6 probably involves the Gd^{III} centers.

b. Properties of Related Materials.[91] The unit cells, melting points, densities, and microhardness of the compounds Ln_3CrS_6 (Ln = all Ln except Pm and Eu) have been determined on polycrystalline samples. From the unit cells it is likely that these sulfides also crystallize in the U_3ScS_6 structure type

P. Ln_4FeS_7 (Ln = Ho,[92] Y[93]) and $Er_{4.6}Mn_{0.4}S_7$[94]

1. Syntheses

The Ln_4FeS_7 compounds were obtained by reacting Fe and Ln_2S_3 at 1373 K under H_2S gas. $Er_{4.6}Mn_{0.4}S_7$ crystals were prepared by reacting MnS and Er_2S_3 at 1273 K with I_2 as a transport agent.

2. Structure

The structure of Ln_4FeS_7 (Figure 20) and $Er_{4.6}Mn_{0.4}S_7$ is of the Y_5S_7 structure type.[93] There are three different cation sites. The first is a seven-coordinate monocapped trigonal-prismatic site oc-

cupied exclusively by Ln^{III} atoms. The other two are octahedral sites that are statistically occupied by Ln^{III} and M^{II} in a 3:1 ratio for Ln_4FeS_7 or in a 4:1 ratio for $Er_{4.6}Mn_{0.4}S_7$. The LnQ_7 prisms and disordered Ln/M-centered octahedra form individual layers along the *a* axis. These layers stack perpendicular to the *c* axis in the order octahedra−octahedra−prisms−octahedra−prisms.

3. Physical Properties

a. Magnetic Properties.[93] Y_4FeS_7 is paramagnetic over the temperature range of 77−673 K, with a μ_{eff} value that corresponds to Fe^{II}.

b. Properties of Related Materials. The magnetic properties of Er_4FeS_7,[93] Ln_4MnS_7 (Ln = Er, Y),[93] and Dy_4MSe_7 (M = Cr−Fe)[95] were measured. The compounds are paramagnetic with μ_{eff} values that correspond to Ln^{III} and M^{II}.

Thermopower measurements on Dy_4MS_7 (M = Cr−Fe)[96] indicate that these compounds are p-type semiconductors.

Q. La_4NiS_7[97]

1. Synthesis

The material was synthesized from a mixture of La_2S_3 and NiS at 1273−1323 K.

2. Structure

This layered compound exhibits an uncharacterized superstructure. However, the subcell is related to that of K_2NiF_4.[98] The La atoms are either seven- or eight-coordinate, whereas the Ni atoms are six- or seven-coordinate (but with two to three long bonds). Both Ni positions are partially occupied as are two of the four S positions.

3. Related Compounds[97]

Unit cell parameters of Ln_4NiS_7 (Ln = Ce, Pr, Nd) and La_4CoS_7 suggest that these materials have the same subcell as La_4NiS_7.

R. $Gd_3Cu_2Te_7$[99]

1. Synthesis

Gd, Cu, and Te were reacted at 1123 K in a KI flux.

2. Structure

The structure of $Gd_3Cu_2Te_7$ (Figure 21) is constructed from $CuTe_4$ tetrahedra, isolated undistorted linear chains of Te atoms, and $GdTe_8$ bicapped trigonal prisms. The $CuTe_4$ tetrahedra form chains by sharing vertices in the *c* direction with a chain of Te atoms, thus forming the central backbone. These chains of tetrahedra also share vertices in the *a* direction to form two-dimensional $^2_\infty[Cu_2Te_5]$ layers. The $GdTe_8$ bicapped trigonal prisms separate the $^2_\infty[Cu_2Te_5]$ layers and isolated Te chains from each other. As is typical for complex polytellurides,[100,101] oxidation states could not be assigned.

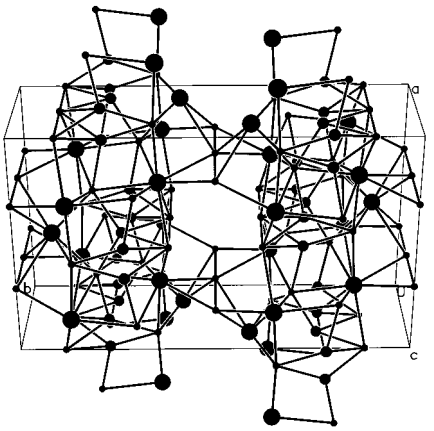

Figure 21. Structure of $Gd_3Cu_2Te_7$.

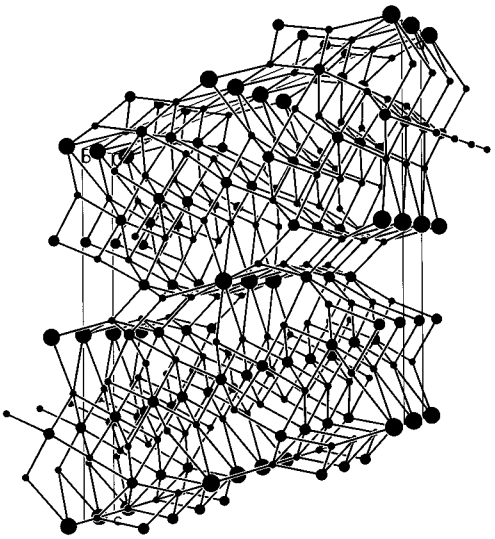

Figure 22. Structure of $Eu_{0.59}Nb_5Se_8$. The Eu sites, which are 59% occupied in the structure, are shown fully occupied.

S. $Eu_{0.59}Nb_5Se_8$[102]

1. Synthesis

The synthesis involved the reaction of the elements at 1275 K.

2. Structure

This three-dimensional structure (Figure 22) comprises two independent Eu atoms, five independent Nb atoms, and eight independent Se atoms. Each of the Eu sites is approximately 59% occupied. The structure is built from several different metal-centered coordination polyhedra: $NbSe_6$ octahedra (two sites), $NbSe_6$ trigonal prisms (three sites), and $EuSe_8$ cubes. The $NbSe_6$ trigonal prisms participate in edge-sharing along the *a* axis to form infinite $NbSe_2$-type chains. Pairs of $NbSe_6$ octahedra connect the chains by sharing faces with the $NbSe_6$ trigonal prisms. Octahedral coordination for Nb is rare, and this coordination geometry produces close Nb−Nb interactions of 2.95(1) Å. Finally, chains of Eu atoms fill the resulting channels by occupying the distorted

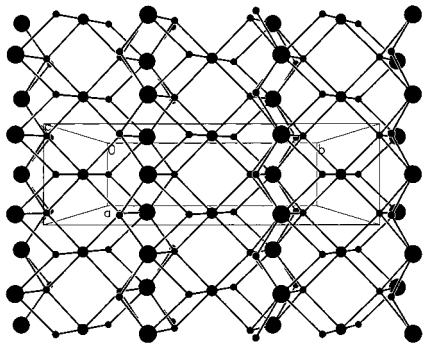

Figure 23. Structure of $Yb_6Fe_2S_{11}$. The cation sites represented by the intermediate-size spheres are statistically occupied by Yb and Fe in a 3:2 ratio.

cubic sites along the *b* axis. Eu in a cubic environment is a rarity.

3. Electrical Conductivity

The material exhibits excellent metallic conductivity along the *b* axis with $\sigma_{298} = 3.5\ 10^4$ and $\sigma_{12} = 1.4\ 10^6$ ohm^{-1} cm^{-1}.

T. $Er_6Cr_2S_{11}$[103] and $Yb_6Fe_2S_{11}$[104]

1. Syntheses

$Er_6Cr_2S_{11}$ was prepared by the reaction of Er_2S_3 and Cr_2S_3 at 1723 K in an atmosphere of H_2S. $Yb_6Fe_2S_{11}$ was prepared from the reaction of FeS and Yb_2S_3 at 1423 K in a current of H_2S.

2. Structure

$Er_6Cr_2S_{11}$ was assigned to space group $Bb2_1m$, an alternative setting of $Cmc2_1$, but was described as having a "pseudo mirror." If the mirror is real, then the space group is *Cmcm*, the group used to describe $Yb_6Fe_2S_{11}$. We take this mirror as being real and these compounds as being isostructural. In this layered structure (Figure 23) there are two independent Ln sites and three independent "M" sites. The Ln sites have a monocapped trigonal-prismatic environment, whereas the "M" sites are octahedral and each consists of a statistical disorder of 60% Yb^{III} and 40% Fe^{II}. The structure comprises rows of LnS_7 prisms linked together by the octahedra.

3. Magnetic Properties of $Er_6Cr_2S_{11}$ and Related Compounds[105]

The compounds $Ln_6Cr_2S_{11}$ (Ln = Gd, Tb, Er, Ho) are paramagnetic in the temperature range 80−300 K. It is not known if the Ln = Gd, Tb, Ho compounds have the same structure as $Er_6Cr_2S_{11}$.

U. $Eu_2Re_6S_{11}$[106]

1. Synthesis

The compound was synthesized by the reaction of Eu_2O_3 with Re in a stream of H_2S at 1523 K.

2. Structure

The structure (Figure 24) contains $[Re_6S_8]$ clusters in which Re_6 octahedra are inscribed in cubes of μ_3-S atoms. It also contains pairs of Eu atoms (Eu···Eu = 3.841(1) Å) in double trigonal prisms that share a triangular face. These polyhedra are linked through S atoms to form the three-dimensional structure.

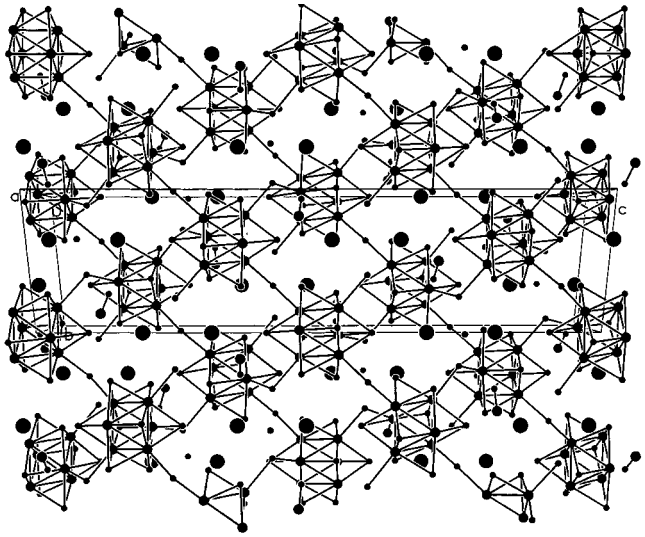

Figure 24. $Eu_2Re_6S_{11}$ structure. The Eu−S bonds have been removed for clarity.

3. Magnetic Properties

The compound is paramagnetic but exhibits an antiferromagnetic transition at 5 K that is ascribed to coupling between the Eu pairs ($J(Eu^{II}-Eu^{II}) = -0.36$ cm^{-1}).

V. $La_{15.9}Cr_{5.4}S_{32}$[107] and $La_{3.266}M_{1.1}S_6$ (M = Mn, Fe)[108,109]

1. Syntheses

$La_{15.9}Cr_{5.4}S_{32}$ was prepared from the reaction of La_2S_3, Cr, and S at 1323 K with $LaCl_3$ as a flux. $La_{3.266}M_{1.1}S_6$ was obtained from the thermal decomposition of La_2MS_4 at 1373 K under a current of H_2S.

2. Structures

The structures of these materials are complicated. $La_{15.9}Cr_{5.4}S_{32}$ contains $[Cr_2S_9^{12-}]$ face-shared bioctahedra that reside on the 3-fold axis of the cell. These bioctahedra are linked alternately by two different M_6S_{13} edge-bridged octahedral cluster units (O and O′). The O clusters are composed entirely of eight-coordinate La atoms with a partially occupied S atom residing in the middle of the cluster. The O′ clusters have both La and Cr disordered on the M sites, making the coordination environment of the cations difficult to ascertain. There is also a partially occupied S atom residing in the middle of the O′ cluster. These three subunits form chains along the *c* axis. These chains are connected to neighboring chains by a seven-coordinate La atom.

The structure of $La_{3.266}M_{1.1}S_6$ is similar to that of $La_{15.9}Cr_{5.4}S_{32}$, although the partially occupied S atom at the center of the O′ cluster in $La_{15.9}Cr_{5.4}S_{32}$ is replaced with three partially occupied M atoms (M = Mn, Fe). Also, the O′ cluster in $La_{3.266}M_{1.1}S_6$ is composed entirely of La atoms.

3. Magnetic Properties

The magnetic susceptibility of $La_{15.9}Cr_{5.4}S_{32}$, measured from 5 to 350 K, supports an all Cr^{III} compound. The compound does not exhibit long-range magnetic interactions, but there is a significant antiferromagnetic coupling between cluster groups.

IV. Quaternary Compounds

The utility of the reactive-flux technique[14] in the synthesis of new quaternary alkali-metal rare-earth d-element chalcogenides (A/Ln/M/Q) has clearly been demonstrated over the past decade. The low melting points of the A_2Q_x fluxes (433−723 K) and their ability to act as both reagent and reaction medium allows for the isolation of species that cannot be obtained by the use of traditional high-temperature solid-state experimental methods. It is likely that in most instances these latter methods yield thermodynamic products whereas the reactive fluxes afford kinetic products.

The dimensional reduction engendered by the addition of an alkali-metal cation to a binary to form a ternary or to a ternary to form a quaternary was documented almost a decade ago.[110] The use of reactive alkali-metal fluxes enables such additions and has generated a host of low-dimensional materials displaying a variety of one-dimensional, layered, and tunnel structures in addition to interesting physical properties. Although the d-element in these systems predominantly has been Cu or Ag, several recent discoveries[111] show that this method can be extended to other transition metals. Reviews are available on the reactive-flux technique[112,113] and on dimensional reduction.[114]

A. $LaPbCuS_3$[115]

1. Synthesis

$LaPbCuS_3$ was synthesized from a mixture of La_2S_3, Pb, Cu, and S at 1273 K.

2. Structure

$LaPbCuS_3$ (Figure 25) is a three-dimensional structure that is closely related to that of α-La_2S_3.[116] The Cu atoms insert into one of the two unoccupied tetrahedral sites of the α-La_2S_3 structure. These CuS_4 tetrahedra form chains parallel to the *b* axis by corner-sharing. Pb^{II} disorders with La^{III} over two crystallographic sites. The La and Pb cations are in a monocapped trigonal-prismatic environment.

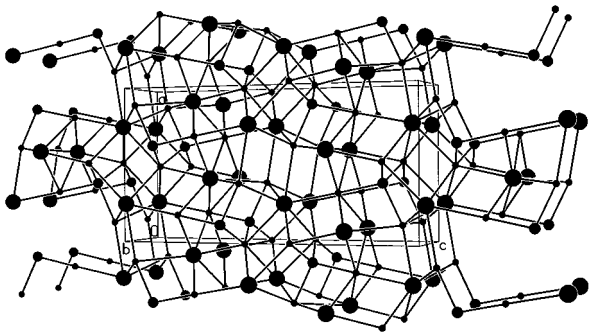

Figure 25. $LaPbCuS_3$ structure. The cation sites represented by the large spheres are statistically occupied by La and Pb.

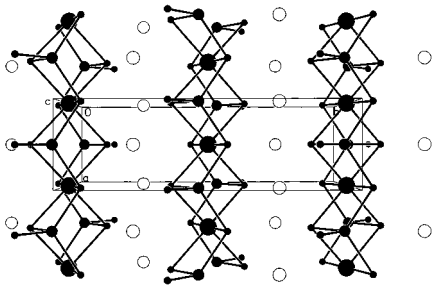

Figure 26. $KZrCuS_3$ structure type, as represented by that of $BaErCuS_3$.

B. $CsCeCuS_3$[117] and $CsGdZnSe_3$[111]

1. Syntheses

$CsCeCuS_3$ was prepared from Ce and Cu with a Cs_2S/S reactive flux at 673 K. $CsGdZnSe_3$ was prepared from the reaction of Gd and Zn with a Cs_2Se_3/Se reactive flux with the addition of CsI as an additional flux at 1273 K.

2. Structures

These compounds possess the $KZrCuS_3$[118] structure type (Figure 26).

3. Physical Properties

$CdGdZnSe_3$[111] is paramagnetic in the range 5−300 K. From a diffuse reflectance spectrum, optical band gaps of 1.88 and 2.92 eV were deduced. The spectrum is indicative of a complex electronic structure involving indirect transitions.

$CsCeCuS_3$[117] has been described as possessing "valence fluctuations." The magnetic response is said to support a $Cs(Cu^{I})(Ce^{III})(S^{II-})_2(S^{-})$ formalism. The conductivity behavior on a pressed polycrystalline pellet is that of a semiconductor. Thermopower measurements indicate holes as the primary charge carriers. Overall, the physical properties of this material are not well understood.

C. $BaLnMQ_3$ Phases

1. Syntheses

Some of the compounds in this large family were synthesized by the reactions of the constituent binary chalcogenides and elements at 1273 K. Others were prepared at 1123 K by the reaction of Ln, M, Q, and BaQ with various fluxes, including $BaBr_2$/KBr and $BaCl_2$.

2. Structures

a. Compounds with the $KZrCuS_3$ Structure Type[118] (Figure 26). These compounds include $BaErCuS_3$,[119] $BaYAgSe_3$,[119] $BaGdAuSe_3$,[48] $BaYCuTe_3$,[48] $BaYAgTe_3$,[48] $BaDyCuTe_3$,[120] and $BaGdCuSe_3$.[111]

This structure comprises $^{2}_{\infty}[LnMQ_3^{2-}]$ layers constructed from MQ_4 tetrahedra and LnQ_6 octahedra. The octahedra share edges in the *a* direction and

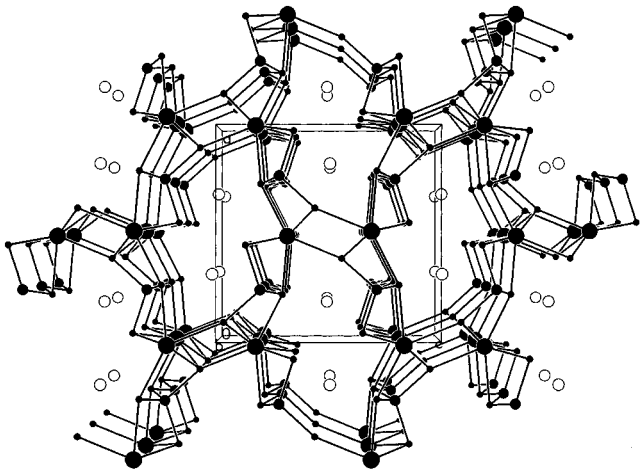

Figure 27. Structure of $BaLaCuS_3$ viewed along the *b* axis.

vertices in the *c* direction to form a two-dimensional $^2_\infty[LnQ_3^{3-}]$ layer. M atoms insert into the vacant tetrahedral sites of the $^2_\infty[LnQ_3^{3-}]$ layers to form $^2_\infty[LnMQ_3^{2-}]$ layers. The coordination of the Ba atoms is either monocapped or bicapped trigonal prismatic, depending on the compound. The Ba atoms reside between the layers.

Powder diffraction patterns indicate that $BaLnCuS_3$ (Ln = Gd, Y),[119] $BaLnCuSe_3$ (Ln = Er, Y),[119] $BaNdAgS_3$,[119] and $BaLnAgSe_3$ (Ln = La, Er)[119] are isostructural with $KZrCuS_3$.

b. Compounds with the Eu_2CuS_3 Structure Type[46] (Figure 12). These include β-$BaLaCuSe_3$[47] and $BaLaCuTe_3$,[48] with La^{III} in place of Eu^{III}, Ba^{II} in place of Eu^{II}, and Se or Te in place of S.

c. Compounds with the $BaLaCuS_3$ Structure Type (Figure 27). These include $BaLaCuS_3$ and α-$BaLaCuSe_3$.[47] $BaLaCuS_3$ has a three-dimensional anionic framework constructed of LaS_7 monocapped trigonal prisms and CuS_4 tetrahedra. The structure has channels that accommodate the Ba atoms.

d. $BaErAgS_3$[121] (Figure 28). This is a three-dimensional tunnel structure that is related to that of $BaLaCuS_3$. The anionic portion of the structure consists of ErS_6 octahedra and AgS_5 units. These AgS_5 polyhedra share corners to form Ag_2S_9 tricapped trigonal bipyramids. The ErS_6 octahedra share edges to form double chains that connect to form the three-dimensional structure through the Ag_2S_9 units.

From powder diffraction data $BaLnAgS_3$ (Ln = Gd, Y)[121] appears to have this structure.

3. Physical Properties

a. Magnetic Properties. Magnetic susceptibilities of a number of these compounds have been measured. All compounds are paramagnetic with effective moments corresponding to Ln^{III}.

b. Optical Properties. Band gaps have been determined from diffuse reflective spectra for $BaYCuS_3$,[119] $BaNdCuS_3$,[119] $BaGdCuS_3$,[119] $BaNdAgS_3$,[119] and $BaGdCuSe_3$.[111] These compounds are semiconductors.

c. Other Properties. β-$BaLaCuSe_3$ converts to α-$BaLaCuSe_3$ upon grinding. The reverse-phase transition occurs when α-$BaLaCuSe_3$ is annealed at elevated temperatures.[47]

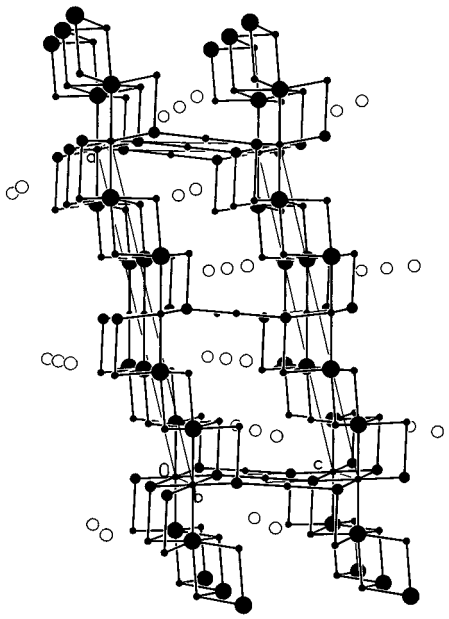

Figure 28. $BaErAgS_3$ structure.

D. $K_{0.5}Ba_{0.5}DyCu_{1.5}Te_3$[120]

1. Synthesis

Ba, Dy, Cu, and Te were reacted at 1123 K in a LiCl/KCl flux.

2. Structure

The structure of $K_{0.5}Ba_{0.5}DyCu_{1.5}Te_3$ is a filled variant of that of the $KZrCuS_3$ structure type (Figure 26).[118] In $K_{0.5}Ba_{0.5}DyCu_{1.5}Te_3$ there is a second Cu site that is partially occupied, ensuring charge balance as Ba is substituted for K. These new Cu atoms also form one-dimensional vertex-sharing chains of tetrahedra that interconnect with adjacent chains to form the three-dimensional structure. Both the Dy and the disordered K/Ba atoms reside in the tunnels formed by this three-dimensional array of $CuTe_4$ tetrahedra. The A, Dy, and Cu atoms are seven-, six-, and four-coordinate, respectively.

E. $KCeCuTe_4$[122]

1. Synthesis

The material was synthesized at 973 K from a reactive K_2Te/Te flux containing Cu and Ce.

2. Structure

The structure (Figure 29) is described as being built from two distinct layers, $^2_\infty[CuTe^-]$ and $^2_\infty[CeTe_3]$, leading to an intergrowth compound with the more descriptive formula $K^+[CuTe^-][CeTe_3]$. The Cu atoms are tetrahedrally coordinated and participate in edge-sharing along the *a* and *b* axes to form $^2_\infty[CuTe^-]$ layers. The Ce atoms are coordinated in tricapped trigonal prisms, and the layers formed from these polyhedra are analogous to the Nd-centered layers of $NdTe_3$.[123] The $^2_\infty[CeTe_3]$ layer contains a square Te

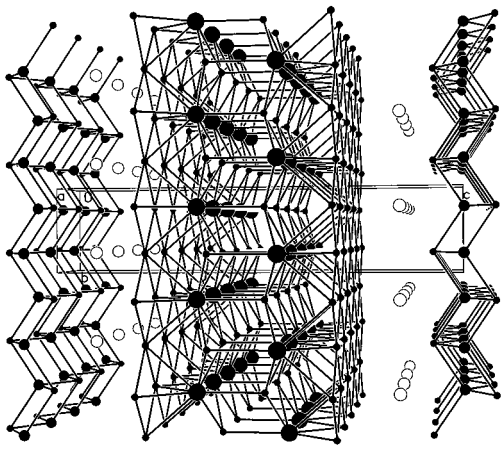

Figure 29. $KCeCuTe_4$ structure.

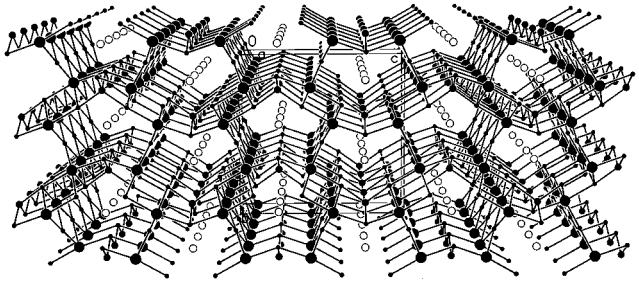

Figure 30. Tunnel structure of the ALn_2CuQ_4 phases, as represented by that of KGd_2CuS_4.

net with a Te−Te distance of 3.1417(6) Å. The $^2_\infty[CuTe^-]$ and $^2_\infty[CeTe_3]$ layers are separated by K atoms and stack alternately along the *c* axis.

3. Physical Properties

The material shows paramagnetic behavior from 5 to 300 K with μ_{eff} corresponding to Ce^{III}. A pellet of $KCeCuTe_4$ shows metallic behavior, and thermopower data suggest that the carriers are holes.

F. ALn_2CuQ_4 Phases

These compounds include KGd_2CuS_4,[124] $RbNd_2CuS_4$,[125] $RbSm_2CuS_4$,[125] $RbSm_2CuSe_4$,[126] $RbGd_2CuSe_4$,[126] $RbDy_2CuSe_4$,[126] $CsLa_2CuSe_4$,[125] and $CsSm_2CuSe_4$.[125]

1. Syntheses

These compounds were synthesized by the reactive-flux method. Details include KGd_2CuS_4[124]−Gd, Cu, K_2S_5/S flux, 723 K; $RbLn_2CuS_4$, Ln = Nd, Sm[125]−Ln, Cu, Rb_2S_3/S flux, 973 K; $RbLn_2CuSe_4$, Ln = Sm, Gd, Dy[126]−Ln, Cu, Rb_2Se_3/Se flux, 1073 K; $CsLn_2CuSe_4$, Ln = La, Sm[125]−Ln, Cu, Cs_2Se_3/Se flux, 973 K.

2. Structure

These compounds are isostructural, crystallizing in the KGd_2CuS_4 structure type (Figure 30). This is a three-dimensional tunnel framework. The tunnels are 10-membered pentagonal rings that are large enough in cross section to accommodate a single eight-coordinate A atom. These AQ_8 polyhedra share triangular faces along the *a* axis. Moreover, the tunnels consist of two Cu−Q bonds and eight Ln−Q bonds. The three-dimensional anionic framework is built from LnQ_6 octahedra and CuQ_4 tetrahedra. The Ln/Q fragments in these compounds consist of distorted $^2_\infty[Ln_2Q_5^{4-}]$ layers that are built from the LnQ_6 octahedra sharing edges parallel to the *a* axis to form chains. The chains are connected through vertex-sharing of Q atoms to form layers. The $^2_\infty[Ln_2Q_5^{4-}]$ layers are connected by the octahedra in one layer sharing edges with octahedra in adjacent layers to form the three-dimensional framework.

G. $K_2CeCu_2S_4$[127]

1. Synthesis

$K_2CeCu_2S_4$ is formed from the reaction of Cu and Ce in a K_2S/S flux at 533 K.

2. Structure

Unfortunately, the atomic coordinates are not available in the original paper or in the deposited material, so we are unable to authenticate the authors' description of the structure, which we paraphrase here. The anionic framework of this layered compound comprises CeS_6 octahedra and CuS_4 tetrahedral. The CeS_6 octahedra share edges along the *b* axis to form chains. The Cu-centered tetrahedra share two edges with octahedra in one chain and a vertex with an octahedron in a neighboring chain to form layers. The K atoms reside in the interlayer gallery.

3. Physical Properties

As for $CsCeCuS_3$,[117] $K_2CeCu_2S_4$ is a p-type semiconductor that has been described as possessing "valence fluctuations". The magnetic response is said to support a $K_2(Cu^I)_2(Ce^{III})(S^{II-})_3(S^-)$ formalism. Overall, the physical properties of this material are not well understood.

H. $KEuCu_2Te_4$[29]

1. Synthesis

A reactive K_2Te/Te flux containing Cu and Eu was used to synthesize the compound at 1123 K.

2. Structure

The structure of $KEuCu_2Te_4$ (Figure 5) is of the $CaMnBi_2$ type[128] and comprises square antiprismatic Eu atoms sandwiched between an *anti*-PbO-type layer of $[CuTe^-]$ and a flat square net of Te atoms. The Cu atoms are tetrahedrally coordinated.

3. Physical Properties

a. Magnetic Properties. $KEuCu_2Te_4$ is paramagnetic over the temperature range 5−300 K; the derived value of μ_{eff} is consistent with Eu^{II}. Attempts to assign formal charges seem strained. It is usually very difficult to assign formal charges in complex tellurides.[100]

b. Transport Properties. Electrical conductivity and thermopower data on a pressed pellet suggest p-type metallic or semimetallic behavior.

4. Related Compound

$Na_{0.2}Ag_{2.8}EuTe_4$[29] is isostructural with $KEuCu_2Te_4$. The compound, prepared at 1123 K from a reactive

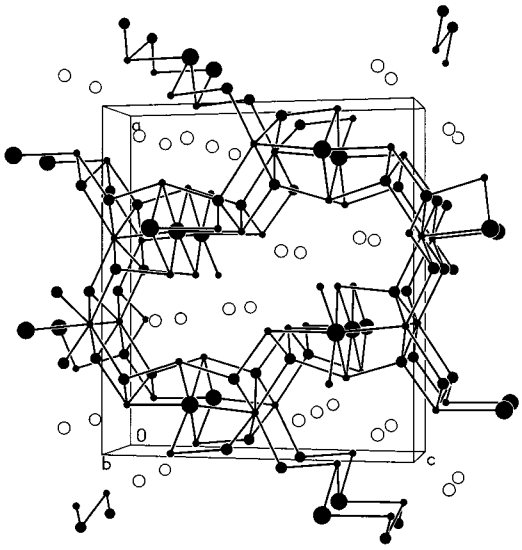

Figure 31. $K_2CeAg_3Te_4$ structure.

Na_2Te/Te flux containing Ag and Eu, is a p-type semiconductor with a band gap of 0.24 eV.

I. $K_2CeAg_3Te_4$[129]

1. Synthesis

This material was synthesized by the reactive-flux technique at 1123 K utilizing a K_2Te/Te flux with added Ag and Ce.

2. Structure

This is a three-dimensional tunnel structure (Figure 31). The tunnels are 16-membered rings that are large enough in cross section to accommodate four K atoms. The anionic framework of $K_2CeAg_3Te_4$ consists of $CeTe_6$ octahedra and $AgTe_4$ tetrahedra. Corrugated $^2_\infty[CeAg_2Te_4^{3-}]$ layers are formed from double rows of edge-sharing $AgTe_4$ tetrahedra that connect with chains of edge-sharing $CeTe_6$ octahedra. These layers are linked by a third Ag atom to form the three-dimensional structure.

3. Physical Properties

The material is paramagnetic in the range 5−300 K, with μ_{eff} consistent with Ce^{III}. $K_2CeAg_3Te_4$ is a p-type semiconductor (band gap = 0.36 eV).

J. $Rb_2CeCu_3Te_5$[130]

1. Synthesis

This material was synthesized from the reaction of Cu and Ce in a Rb_2Te/Te reactive flux at 1123 K.

2. Structure

This compound has a layered structure (Figure 32). The Ce atom is coordinated in a distorted pentagonal bipyramid in which one η^2-Te_2^{2-} unit and three Te^{2-} anions comprise the pentagon and the two Te^{2-}units are in the axial positions. These bipyramids share Te^{2-} units to form chains along the *b* axis. Cu atoms occupy the tetrahedral positions within these chains. Each $CuTe_4$ tetrahedron is coordinated at two vertices to the axial positions on two neighboring

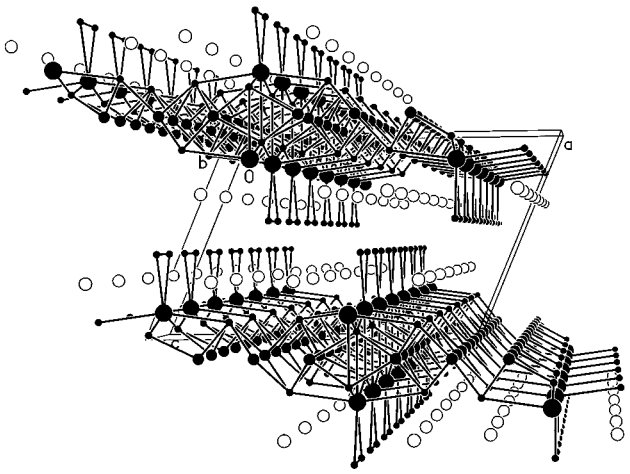

Figure 32. Structure of $Rb_2CeCu_3Te_5$ viewed down the *b* axis.

pentagonal bipyramids and at the remaining vertices to the closest edge between these axial positions. The $^1_\infty[CeCu_2Te_5^{3-}]$ chains connect by means of a second type of distorted $CuTe_4$ tetrahedron to form $^1_\infty[CeCu_3Te_5^{2-}]$ layers along the *a* axis. As is typical for these compounds, the Rb atoms reside between the anionic layers.

3. Physical Properties

The compound is paramagnetic in the range 5−300 K with a μ_{eff} consistent with Ce^{III}. From electrical conductivity and thermopower measurements the material is a p-type semiconductor with a narrow band gap.

K. $ALn_2M_3Q_5$ Phases

These compounds include $RbEr_2Cu_3S_5$,[125] $CsGd_2Ag_3Se_5$,[125] $CsTb_2Ag_3Se_5$,[125] and $RbSm_2Ag_3Se_5$.[126]

1. Syntheses

These compounds were synthesized by the reactive-flux method at 973 or 1073 K. Ln and M were added to a reactive flux of A_2Q_3/Q.

2. Structure

These isostructural compounds crystallize in the $RbSm_2Ag_3Se_5$ structure type, a three-dimensional tunnel structure (Figure 33). The tunnels are 10-membered pentagonal rings consisting of six Cu−Q bonds and four Ln−Q bonds that are large enough in cross section to accommodate a single eight-coordinate A atom. These AQ_8 polyhedra share triangular faces along the *a* axis. The three-dimensional anionic framework is built from LnQ_6 octahedra and CuQ_4 tetrahedra. The Ln/Q fragments in these compounds consist of distorted $^2_\infty[Ln_2Q_5^{4-}]$ layers that are built from the LnQ_6 octahedra sharing edges parallel to the *a* axis to form chains. The chains connect through vertex-sharing of Q atoms to form layers. In contrast, the MQ_4 tetrahedra share vertices and edges to form two-dimensional layers that connect to form the tunnel structure. The tunnels in this structure are very similar to those in ALn_2CuQ_4 (Figure 30).

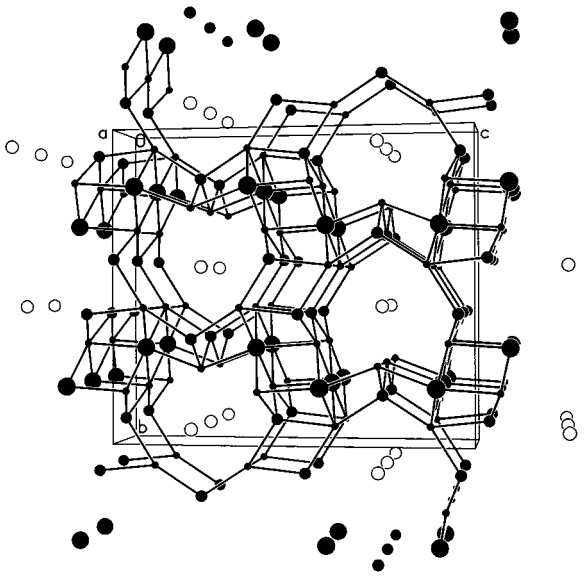

Figure 33. Structure of $RbSm_2Ag_3Se_5$, which is adopted by the $ALn_2M_3Q_5$ phases.

3. Physical Properties

$RbEr_2Cu_3S_5$ is paramagnetic between 5 and 300 K; the derived value of μ_{eff} is consistent with Er^{III}. The compound exhibits a typical Er^{III} absorption spectrum, with 4f−4f transitions at about 1.6, 1.9, and 2.5 eV.

L. ALn_2CuQ_6 Phases

This family includes KCe_2CuS_6,[127] KCe_2CuSe_6,[117,131] KEu_2CuS_6,[132] and $CsCe_2CuS_6$.[117]

1. Syntheses

All four compounds were synthesized by the reactive-flux method. KCe_2CuS_6[127] was synthesized by the reaction of K_2S, Cu, Ce, and S at 543 K. KCe_2CuSe_6[131] was synthesized by the reaction of K_2Se, Cu, Ce, and Se at 723 K. KEu_2CuS_6[132] was synthesized at 653 K by reacting K_2S_3 with Cu, EuS, and S. $CsCe_2CuS_6$[117] was synthesized from Cs_2S, Cu, Ce, and S at 673 K.

2. Structures

Phases with this stoichiometry were originally reported to crystallize in several different space groups—KCe_2CuS_6[127] in $C2/c$, $CsCe_2CuS_6$ and KCe_2CuSe_6[117] in $Immm$, and KEu_2CuS_6[132] in $Fddd$. It was later shown that the earlier work was incorrect and that KCe_2CuSe_6[131] actually crystallizes in $Fddd$. That work also indicated a possible orthorhombic cell for KCe_2CuS_6. In any event, the structures of these four compounds are essentially the same (Figure 34), possibly differing in the ordering of the Cu sites. The structure consists of anionic layers formed from LnQ_8 and CuQ_4 polyhedra with A atoms residing between the layers. In these compounds the Ln atoms are coordinated to two Q_2^{2-} units and four Q^{2-} anions to form a bicapped trigonal prism. The Q_2^{2-} units form the short side of the prism, whereas the Q^{2-} anions occupy the apex and capping positions. These prisms share triangular faces in the *a* direction to form chains. Layers are then formed when neighboring chains share Q^{2-} units, such that the capping unit of one prism is the third Q atom of the triangular face of a neighboring LnQ_8 polyhedron. The Ln/Q portion of this structure is analogous to several known phases, including $ZrSe_3$[133] and $CsTh_2Te_6$.[134] The Ln-centered prismatic chains possess tetrahedral sites that accommodate the Cu^+ ions. The CuQ_4 tetrahedra are coordinated to the ends of two separate Q_2^{2-} units and to Q^{2-} units at the remaining sites. The A atoms are eight coordinate and connect the anionic layers together parallel to the *c* axis.

3. Physical Properties

a. Optical Properties. From diffuse reflectance measurements the band gaps of KCe_2CuS_6[127] and $CsCe_2CuS_6$[117] are 1.8 and 2.0 eV, respectively. A band gap of 0.55 eV is estimated for KCe_2CuSe_6.[117]

b. Magnetic Properties. $CsCe_2CuS_6$[117] is paramagnetic between 2 and 300 K and shows some local antiferromagnetic ordering at low temperatures. KCe_2CuS_6[127] is paramagnetic above 160 K. These magnetic data are consistent with Ce^{III}.

4. Related Compounds

From X-ray powder data KLa_2CuS_6[117] appears to be related structurally to this family of compounds.

M. $Ba_2LnAg_5S_6$ (Ln = La, Y)[135]

1. Syntheses

These compounds were prepared by the reaction of BaS, La_2S_3 or Y_2S_3, Ag, and S at 1273 K.

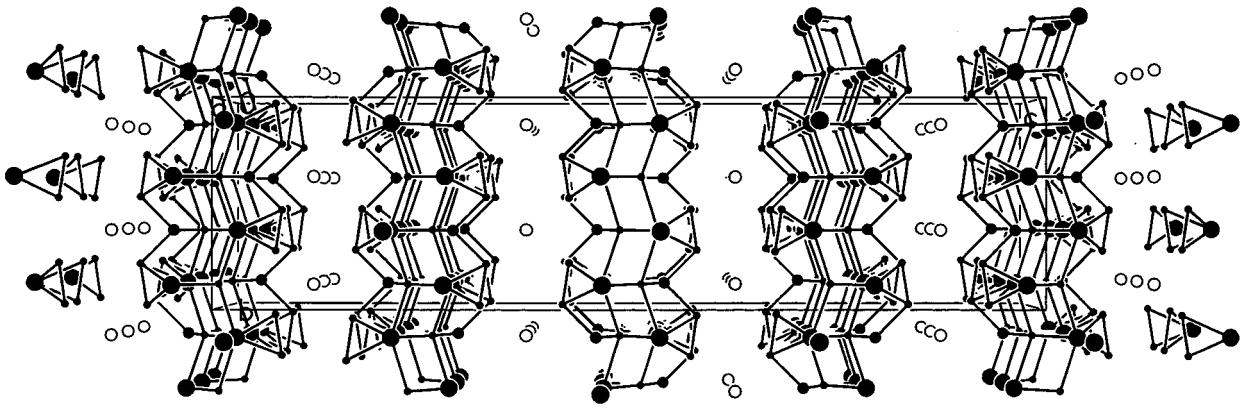

Figure 34. Structure of KEu_2CuS_6 viewed along the *a* axis.

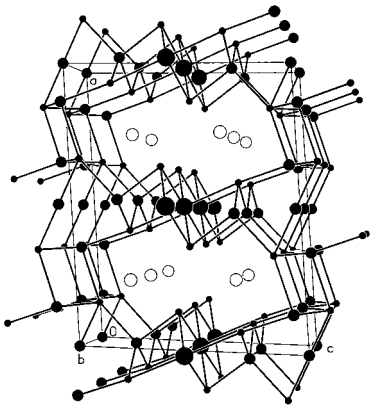

Figure 35. $Ba_2LnAg_5S_6$ structure, as typified by that of $Ba_2LaAg_5S_6$.

2. Structure

The three-dimensional tunnel framework of $Ba_2LnAg_5S_6$ (Figure 35) is built from LnS_6 octahedra, AgS_4 tetrahedra (two unique crystallographic sites), and linear AgS_2 units (one crystallographic site). The AgS_2 unit can also be thought of as a highly compressed octahedron, consisting of the two bonded S atoms and the four next-nearest S neighbors. However, these next-nearest neighbors are at a Ag···S distance of 3.841(3) Å, much too long to be bonding. Ba atoms are accommodated in the tunnels.

3. Related Compound

From X-ray film photography, $Ba_2YAg_5S_6$ appears to be isostructural with $Ba_2LaAg_5S_6$.

N. La_3CuSiS_7[136]

La_3CuSiS_7 is a member of a very large family of compounds crystallizing in the hexagonal system, the first to be studied by single-crystal diffraction methods being $Ce_6Al_{3.33}S_{14}$.[137] Since this material crystallizes in a polar space group, it should exhibit piezoelectric and second-order nonlinear optical behavior. For this reason many new phases have been synthesized. This family now consists of over 250 compounds.[136] Although the majority of this work was completed prior to 1970, there have been several recent additions.[138−140] For the sake of brevity, only the structure La_3CuSiS_7[136] will be discussed here. A more detailed description of these materials is available.[136]

1. Synthesis

La_3CuSiS_7 was obtained from a mixture of La_2S_3 and Cu_2S at 1473 K under an atmosphere of H_2S charged with SiS_2 vapor.

2. Structure

This three-dimensional compound (Figure 36) crystallizes in the space group $P6_3$. The La atoms are eight-coordinate in a bicapped trigonal-prismatic environment. The Cu atoms sit on the hexagonal axis in a severely distorted octahedral environment with three short Cu−S bonds and three long Cu−S interactions. This bonding environment may more accurately be described as CuS_3 triangles. The Si atom is on the 3-fold axis and is tetrahedrally coordinated. In this structure the LaS_8 prisms share corners along the *c* axis to form chains. The isolated CuS_3 triangles and SiS_4 tetrahedra pack parallel to the *c* axis in vacancies created by the La-centered chains.

3. Physical Properties[136]

A strong piezoelectric effect is observed for La_3CuSiS_7.

4. Physical Properties of Related Compounds

Magnetic measurements on La_3MAlS_7 (M = Mn−Co)[141] show that these materials are antiferromagnetic with Néel temperatures between 110 and 130 K. However, a neutron diffraction study on La_3MnAlS_7[142] indicated that there is no long-range magnetic order down to 1.2 K. The reason for this discrepancy is unknown.

The La_3MFeS_7 (M = Fe−Ni, Zn)[141] materials are all p-type semiconductors, with the exception of the Ni compound which is metallic. Among these materi-

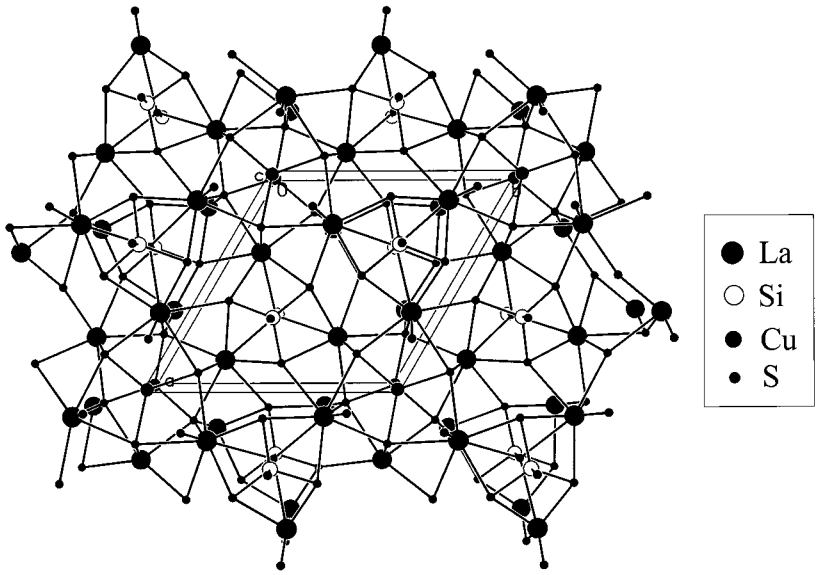

Figure 36. Structure of La_3CuSiS_7.

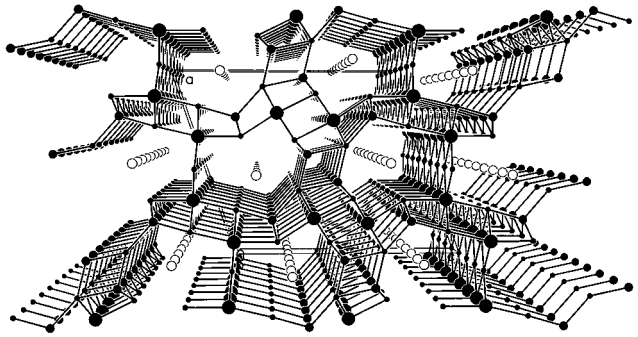

Figure 37. Structure of $Rb_2Gd_4Cu_4S_9$ viewed along the *b* axis.

als only $La_3Fe_2S_7$ orders magnetically; it shows an antiferromagnetic transition at 155 K.[142] Both the Fe-centered octahedra and tetrahedra participate in the magnetic ordering.

O. $Rb_2Gd_4Cu_4S_9$[125]

1. Synthesis

The compound was synthesized at 973 K by the addition of Gd and Cu to a reactive Rb_2S_3/S flux.

2. Structure

This compound possesses a three-dimensional tunnel framework structure (Figure 37). Each tunnel consisting of four Cu−S bonds and six Gd−S bonds is a 10-membered pentagonal ring that is large enough in cross section to accommodate a single eight-coordinate Rb atom. These RbS_8 polyhedra share triangular faces along the *a* axis. The three-dimensional anionic framework in this structure is built from GdS_6 octahedra and CuS_4 tetrahedra. The Gd/S fragments consist of distorted $^2_\infty[Gd_2S_5^{4-}]$ layers that are built from the GdS_6 octahedra sharing edges parallel to the *a* axis to form chains. The chains connect through vertex-sharing of S atoms to form layers. The $^2_\infty[Gd_2S_5^{4-}]$ layers connect by an octahedron in one layer sharing edges with octahedra in adjacent layers to form the three-dimensional framework. The tunnels in this structure have shapes similar to those in $ALn_2M_3Q_5$ (Figure 33) and ALn_2CuQ_4 (Figure 30).

3. Physical Properties

The material is paramagnetic in the temperature range 5−300 K; the derived value of μ_{eff} is consistent with Gd^{III}. A band gap of 1.94 eV has been deduced from a diffuse reflectance spectrum.

P. $Ba_4Ln_2Cd_3Q_{10}$

This family includes $Ba_4Ln_2Cd_3S_{10}$ (Ln = Sm, Gd, Tb)[143] and $Ba_4Nd_2Cd_3Se_{10}$.[143]

1. Syntheses

The materials were prepared by the reaction of stoichiometric amounts Ln, Cd, Q, and BaQ in a $BaBr_2$/KBr eutectic flux at 1173 K.

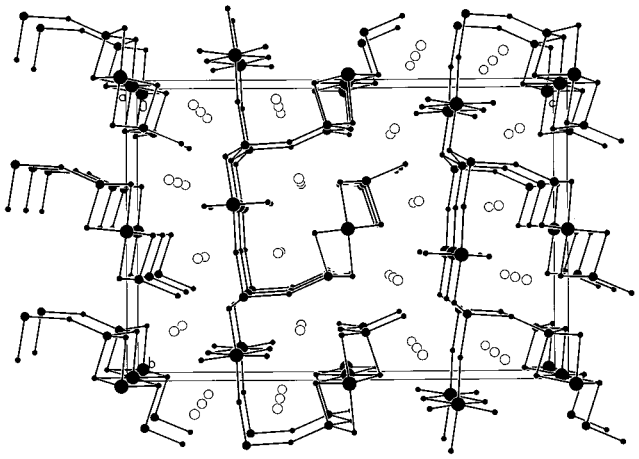

Figure 38. Structure of the $Ba_4Ln_2Cd_3Q_{10}$ compounds, as represented by that of $Ba_4Nd_2Cd_3Se_{10}$.

2. Structure

The structure of these compounds (Figure 38) is composed of two-dimensional $^2_\infty[Ln_2Cd_3Q_{10}^{8-}]$ layers that stack perpendicular to the *c* axis. The $^2_\infty[Ln_2Cd_3Q_{10}^{8-}]$ layers consist of chains of edge-sharing LnQ_6 octahedra and vertex-sharing CdQ_4 tetrahedra that share vertices with each other along the *b* axis. Additionally, there are branching planes of $CdQ_4-LnQ_6-CdQ_4$ units that stick out of the main plane. The Ba atoms, which reside between the layers, adopt two coordination environments, a monocapped and a bicapped trigonal prism.

3. Physical Properties

$Ba_4Tb_2Cd_3S_{10}$ is paramagnetic over the temperature range 2−300 K; the derived value of μ_{eff} is consistent with Tb^{III}. A band gap of 3.0 eV was deduced for this compound from a diffuse reflectance spectrum.

Q. $A_3Ln_4Cu_5Q_{10}$ Phases

Compounds in this series include $K_3Dy_4Cu_5Te_{10}$,[120] $Rb_3Ln_4Cu_5Se_{10}$ (Ln = Gd, Dy),[126] $K_3Ln_4Cu_5Te_{10}$ (Ln = Sm, Gd, Er),[144] $Rb_3Ln_4Cu_5Te_{10}$ (Ln = Nd, Gd),[144] and $Cs_3Gd_4Cu_5Te_{10}$.[144]

1. Syntheses

The selenides were synthesized by the reactive-flux method at 1073 K from Rb_2Se_3/Se with added Ln and Cu. The tellurides were synthesized at 1123 from Ln, Cu, and Te in a LiCl/ACl flux.

2. Structures

These three-dimensional tunnel structures are illustrated in Figure 39 for $Rb_3Dy_4Cu_5Se_{10}$. All nine compounds crystallize in the same space group and have very similar structures built from $LnTe_6$ octahedra and $CuTe_4$ tetrahedra. These structures differ mainly in the location of the Cu3 atom. The four Cu sites in these compounds are illustrated in Figure 40. Atoms Cu1 and Cu2 are always in Sites I and II, respectively. The Cu3 atom in $K_3Ln_4Cu_5Te_{10}$ (Ln = Sm, Gd, Er) is located in Site III, and the Cu3 and Cu4 atoms in $K_3Dy_4Cu_5Te_{10}$ are disordered over Sites

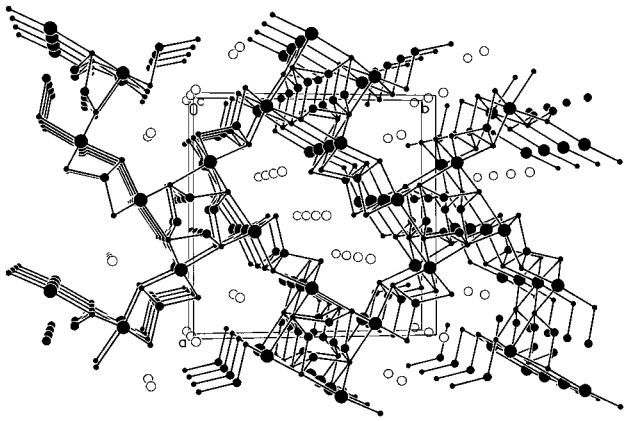

Figure 39. Structure of the $A_3Ln_4Cu_5Q_{10}$ phases, as represented by that of $Rb_3Dy_4Cu_5Se_{10}$.

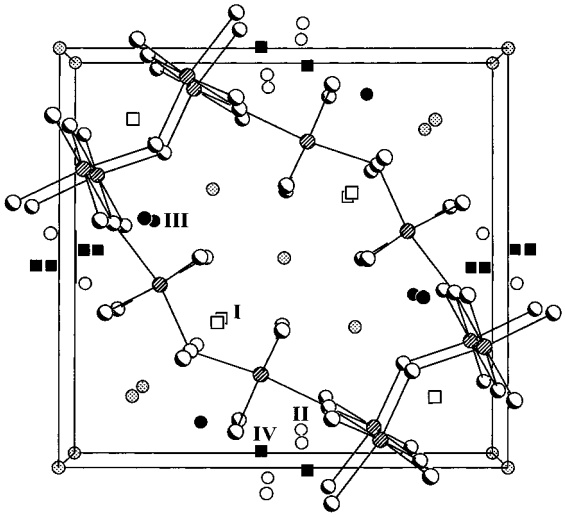

Figure 40. Common fragment of the $A_3Ln_4Cu_5Q_{10}$ structure viewed down the *c* axis. The four Cu sites (I, II, III, IV) are shown, but the Cu−Q and A−Q bonds are not.

III and IV. The Cu3 atom in $Rb_3Ln_4Cu_5Se_{10}$ (Ln = Gd, Dy), $Rb_3Ln_4Cu_5Te_{10}$ (Ln = Nd, Gd), and $Cs_3Gd_4Cu_5Te_{10}$ is located in Site IV, but in $Rb_3Ln_4Cu_5Se_{10}$ both the Cu2 and Cu3 sites are partially occupied. The tunnel in $K_3Ln_4Cu_5Te_{10}$ (Ln = Sm, Gd, Er) contains three K^+ cations in a 16-membered ring comprising eight Cu−Te bonds and eight Ln-Te bonds. The tunnel (Figure 39) in $Rb_3Ln_4Cu_5Te_{10}$ (Ln = Nd, Gd), $Cs_3Gd_4Cu_5Te_{10}$, $Rb_3Ln_4Cu_5Se_{10}$ (Ln = Gd, Dy), and $K_3Dy_4Cu_5Te_{10}$ contains three A^+ cations in a 20-membered ring comprising four Cu−Q bonds and 16 Ln−Q bonds.

3. Magnetic Properties[126]

$Rb_3Dy_4Cu_5Se_{10}$ is paramagnetic in the range 5−300 K with a μ_{eff} corresponding to Dy^{III}.

R. $Ln_8CrTe_{13}Cl$ (Ln = Sm, Gd, Tb)[145]

1. Syntheses

These compounds were synthesized by the reaction of Ln, Cr, Te, and $CrCl_3$ at 1123 K.

2. Structure

The structure (Figure 41) has been described as a pseudo-misfit-layer structure. It consists of alternating rock-salt and CdI_2-type layers with the compositions $[Ln_6Te_5Cl]$ and $[Ln_2CrTe_6]$, respectively. The structure differs from that of typical misfits because the Ln−Te bonds connect the layers and because in the CdI_2-type layer the hexagonal closest-packed sheets are distorted.

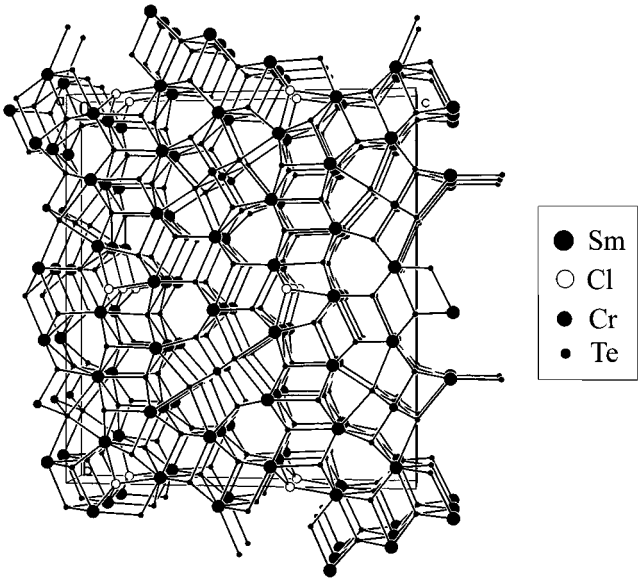

Figure 41. $Ln_8CrTe_{13}Cl$ structure type as typified by that of $Sm_8CrTe_{13}Cl$. Here the unfilled spheres represent Cl atoms.

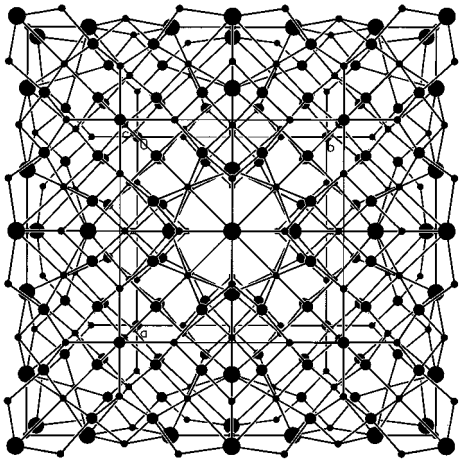

Figure 42. Structure of $Eu_6Cu_{12}Fe_{13}S_{27}$. The intermediate-size spheres represent both the Cu and the Fe atoms.

The coordination of the eight independent Ln atoms comprise three 7-octahedra and five bicapped trigonal prisms. The Cr atom is in a slightly distorted octahedron of Te atoms.

S. $Eu_6Cu_{12}Fe_{13}S_{27}$[146]

1. Synthesis

The compound was prepared from EuS and $FeCuS_2$ at 1173 K under CS_2/Ar.

2. Structure

$Eu_6Cu_{12}Fe_{13}S_{27}$ (Figure 42) is isostructural with $Ba_6Cu_{12}Fe_{13}S_{27}$.[147] The structure consists of Fe- and Cu-centered tetrahedra that share edges and corners

to form a three-dimensional cubic framework. The tetrahedra form large interconnecting tunnels and octahedral cages. Within each unit cell a FeS_6 and an Eu_6S octahedron occupy these tunnels and cages, respectively. Alternatively, the Eu cations may be thought of as being coordinated to nine S atoms in a tricapped trigonal-prismatic arrangement. In this material Fe is present in both the +II and +III oxidation states, and the formula of this compound may be written as $Eu^{II}_6Cu^{I}_{12}Fe^{II}_9Fe^{III}_4S^{II}_{27}$.

V. Conclusions

Although many compounds have been mentioned in this review of rare-earth transition-metal chalcogenides, numerous additional compounds remain to be discovered and studied. It is obvious that with current synthetic techniques, such as the use of reactive fluxes, new phases can be isolated. The rich structural chemistry of this still developing field is dominated by 3d/4f sulfides. Information on possible selenide and telluride analogues of these compounds is largely lacking. Experience suggests that these selenides and especially tellurides will not be "analogues" but will have different structure types and different physical properties. Information on 4d/4f and 5d/4f chalcogenides is sorely lacking. Consistent studies across both the Ln and M series for a given structure type are practically nonexistent at present but are essential if correlations between structure and physical properties are to be drawn. Additional optical, transport, and magnetic measurements, combined with improved theoretical calculations, are needed for most of the compounds discussed in this review. Additionally, more sophisticated magnetic measurements and neutron diffraction studies are essential if we are to catalog and understand the highly sought-after d/f magnetic interactions.

VI. Abbreviations

Ln	rare-earth metal or Y
Q	S, Se, or Te
M	transition metal, excluding Sc
T	main-group element
A	alkali or alkaline-earth metal

VII. Acknowledgments

This research was supported by NSF Grant DMR00-96676 and a Ford Foundation Predoctoral Fellowship to K.M. We thank Ismail Ijjali and Hannah Storrie for their help in translating some references.

VIII. References

(1) Fischer, O. *Springer Ser. Solid-State Sci.* **1990**, *90*, 96−112.
(2) Prodan, A.; Marinkovic, V.; Boswell, F. W.; Bennett, J. C.; Remskar, M. *J. Alloys Compd.* **1995**, *219*, 69−72.
(3) West, A. R. *Basic Solid State Chemistry*, 2nd ed.; John Wiley & Sons: Ltd.: New York, 1999.
(4) Hautala, J.; Taylor, P. C. *J. Non-Cryst. Solids* **1992**, *141*, 24−34.
(5) Tritt, T. M. *Science* **1999**, *283*, 804−805.
(6) Wohlfarth, E. P. In *Ferromagnetic Materials*; Wohlfarth, E. P., Ed.; North-Holland: New York, 1980; Vol. 1, pp 1−70.
(7) Givord, D.; Courtois, D. *J. Magn. Magn. Mater.* **1999**, *196−197*, 684−688.
(8) Solymar, L.; Walsh, D. *Electrical Properties of Materials*, 6th ed.; Oxford University Press: New York, 1998.
(9) Lunn, B.; Davies, J. J. *Semicond. Sci. Technol.* **1990**, *5*, 1155−1160.
(10) Helszan, J. *YIG Resonators and Filters*; John Wiley & Sons: New York, 1985.
(11) Herbst, J. F. *Rev. Mod. Phys.* **1991**, *63*, 819−898.
(12) Raymond, S.; Rueff, J. P.; Shapiro, S. M.; Wochner, P.; Sette, F.; Lejay, P. *Solid State Commun.* **2001**, *118*, 473−477.
(13) Goldman, A. I.; Stassis, C.; Canfield, P. C.; Zaretsky, J.; Dervenagas, P.; Cho, B. K.; Johnston, D. C.; Sternlieb, B. *Phys. Rev. B* **1994**, *50*, 9668−9671.
(14) Sunshine, S. A.; Kang, D.; Ibers, J. A. *J. Am. Chem. Soc.* **1987**, *109*, 6202−6204.
(15) Rouxel, J.; Meerschaut, A.; Wiegers, G. A. *J. Alloys Compd.* **1995**, *229*, 144−157.
(16) Narducci, A. A.; Ibers, J. A. *Chem. Mater.* **1998**, *10*, 2811−2823.
(17) Julien-Pouzol, M.; Jaulmes, S.; Mazurier, A.; Guittard, M. *Acta Crystallogr., Sect. B: Struct. Crystallogr. Cryst. Chem.* **1981**, *37*, 1901−1903.
(18) Guseinov, G. G.; Amirov, A. S.; Amiraslanov, I. R.; Mamedov, K. S. *Dokl. Akad. Nauk Az. SSR* **1984**, *40*, 62−64.
(19) Lauxmann, P.; Schleid, T. *Z. Anorg. Allg. Chem.* **2000**, *626*, 1608−1612.
(20) Huang, F. Q.; Ibers, J. A. *Inorg. Chem.* **1999**, *38*, 5978−5983.
(21) Murugesan, T.; Gopalakrishnan, J. *Indian J. Chem., Sect. A* **1983**, *22*, 469−474.
(22) Ballestracci, R. *C. R. Seances Acad. Sci., Ser. C* **1966**, *262*, 1253−1256.
(23) Julien-Pouzol, M.; Guittard, M. *Bull. Soc. Chim. Fr.* **1968**, 2293−2295.
(24) Julien-Pouzol, M.; Guittard, M. *C. R. Seances Acad. Sci., Ser. C* **1969**, *269*, 316−319.
(25) Julien-Pouzol, M.; Guittard, M. *Ann. Chim. (Paris)* **1973**, *8*, 139−145.
(26) Julien-Pouzol, M.; Laruelle, P. *Acta Crystallogr., Sect. B: Struct. Crystallogr. Cryst. Chem.* **1977**, *33*, 1510−1512.
(27) van der Lee, A.; van de Belt, R.; Wiegers, G. A. *J. Alloys Compd.* **1992**, *178*, 57−70.
(28) Pardo, M.-P.; Julien-Pouzol, M.; Flahaut, J. *C. R. Seances Acad. Sci., Ser. C* **1973**, *276*, 599−602.
(29) Patschke, R.; Brazis, P.; Kannewurf, C. R.; Kanatzidis, M. G. *J. Mater. Chem.* **1999**, *9*, 2293−2296.
(30) Dung, N.-H.; Pardo, M.-P.; Boy, P. *Acta Crystallogr., Sect. C: Cryst. Struct. Commun.* **1983**, *39*, 668−670.
(31) Huang, F. Q.; Brazis, P.; Kannewurf, C. R.; Ibers, J. A. *J. Am. Chem. Soc.* **2000**, *122*, 80−86.
(32) Pardo, M.-P.; Gardette, M.-F.; Flahaut, J. *J. Solid State Chem.* **1991**, *90*, 1−7.
(33) Pardo, M.-P.; Dung, N. H. *C. R. Acad. Sci. Paris* **1987**, *12*, 637−639.
(34) Onoda, M.; Chen, X.-an; Sato, A.; Wada, H. *J. Solid State Chem.* **2000**, *152*, 332−339.
(35) Guymont, M.; Tomas, A.; Julien-Pouzol, M.; Jaulmes, S.; Guittard, M. *Phys. Status Solidi A* **1990**, *121*, 21−28.
(36) Bestaoui, N.; Herle, P. S.; Corbett, J. D. *J. Solid State Chem.* **2000**, *155*, 9−14.
(37) Kwon, Y.-U.; Sevov, S. C.; Corbett, J. D. *Chem. Mater.* **1990**, *2*, 550−556.
(38) Maggard, P. A.; Corbett, J. D. *J. Am. Chem. Soc.* **2000**, *122*, 10740−10741.
(39) Meng, F.; Hughbanks, T. *Inorg. Chem.* **2001**, *40*, 2482−2483.
(40) Muller, O.; Roy, R. *The Major Ternary Structural Families*; Springer-Verlag: Berlin, 1974; pp 209−210.
(41) Huy-Dung, N.; Étienne, J.; Laruelle, P. *Bull. Soc. Chim. Fr.* **1971**, 2433−2437.
(42) Kurbanov, T. K.; Rustamov, P. G.; Aliev, O. M.; Aliev, I. P. *Inorg. Mater. (Transl. of Neorg. Mater.)* **1977**, *13*, 605−606.
(43) Mar, A.; Ibers, J. A. *Acta Crystallogr., Sect. C: Cryst. Struct. Commun.* **1992**, *48*, 771−773.
(44) Gorochov, O.; Barthélemy, E.; Dung, N. H. *C. R. Seances Acad. Sci., Ser. C* **1971**, *273*, 368−371.
(45) Gorochov, O.; McKinzie, H. *J. Solid State Chem.* **1973**, *7*, 400−407.
(46) Lemoine, P.; Carré, D.; Guittard, M. *Acta Crystallogr., Sect. C: Cryst. Struct. Commun.* **1986**, *42*, 390−391.
(47) Christuk, A. E.; Wu, P.; Ibers, J. A. *J. Solid State Chem.* **1994**, *110*, 330−336.
(48) Yang, Y.; Ibers, J. A. *J. Solid State Chem.* **1999**, *147*, 366−371.
(49) Tomas, A.; Shilo, I.; Guittard, M. *Mater. Res. Bull.* **1978**, *13*, 857−859.
(50) Tomas, A.; Tien, V.; Guittard, M.; Flahaut, J.; Guymont, M. *Mater. Res. Bull.* **1985**, *20*, 1027−1030.
(51) Tomas, A.; Guittard, M.; Flahaut, J.; Guymont, M.; Portier, R.; Gratias, D. *Acta Crystallogr., Sect. B: Struct. Crystallogr. Cryst. Chem.* **1986**, *42*, 364−371.
(52) Ben-Dor, L.; Shilo, I.; Felner, I. *J. Solid State Chem.* **1979**, *28*, 363−367.
(53) Tomas, A.; Brossard, L.; Guittard, M. *J. Solid State Chem.* **1980**, *34*, 11−16.

(54) Range, K.-J.; Eglmeier, C. *J. Alloys Compd.* **1991**, *176*, L13−L16.
(55) Longo, J. M.; Raccah, P. M. *Mater. Res. Bull.* **1967**, *2*, 541−547.
(56) Suchow, L.; Ando, A. A. *J. Solid State Chem.* **1970**, *2*, 156−159.
(57) Kainuma, S. *J. Phys. Soc. Jpn.* **1971**, *30*, 1205−1206.
(58) Pawlak, L.; Duczmal, M. *J. Alloys Compd.* **1992**, *184*, 203−209.
(59) Ben-Dor, L.; Shilo, I. *J. Solid State Chem.* **1980**, *35*, 103−106.
(60) Fujii, H.; Okamoto, T. *J. Phys. Soc. Jpn.* **1972**, *32*, 1432.
(61) Pokrzywnicki, S.; Pawlak, L.; Czopnik, A. *Physica B* **1977**, *86−88*, 1141−1142.
(62) Yim, W. M.; Fan, A. K.; Stofko, E. J. *J. Electrochem. Soc.* **1973**, *120*, 441−446.
(63) Agaev, A. B.; Rustamov, P. G.; Aliev, O. M.; Azadaliev, R. A. *Inorg. Mater. (Transl. of Neorg. Mater.)* **1989**, *25*, 250−254.
(64) Aliev, O. M.; Agaev, A. B.; Azadaliev, R. A. *Inorg. Mater. (Transl. of Neorg. Mater.)* **1997**, *33*, 1123−1127.
(65) Lemoine, P.; Tomas, A.; Vovan, T.; Guittard, M. *Acta Crystallogr., Sect. C: Cryst. Struct. Commun.* **1990**, *46*, 365−368.
(66) Vincent, H.; Bertaut, E. F.; Baur, W. H.; Shannon, R. D. *Acta Crystallogr., Sect. B: Struct. Crystallogr. Cryst. Chem.* **1976**, *32*, 1749−1755.
(67) Vollebregt, F. H. A.; Ijdo, D. J. W. *Acta Crystallogr., Sect. B: Struct. Crystallogr. Cryst. Chem.* **1982**, *38*, 2442−2444.
(68) Agaev, A. B.; Rustamov, P. G.; Mamedova, L. M. *Dokl. Akad. Nauk Az. SSR* **1988**, *44*, 41−43.
(69) Flahaut, J. In *Handbook on the Physics and Chemistry of Rare Earths*; Gschneidner, K. A., Jr., Eyring, L. R., Eds.; North-Holland: New York, 1979; Vol. 4, pp 1−88.
(70) Patrie, M.; Chevalier, R. *C. R. Seances Acad. Sci., Ser. C* **1966**, *263*, 1061−1064.
(71) Ben-Dor, L.; Shilo, I. *J. Solid State Chem.* **1980**, *35*, 99−102.
(72) Heikens, H. H.; Kuindersma, R. S.; van Bruggen, C. F.; Haas, C. *Phys. Status Solidi A* **1978**, *46*, 687−695.
(73) Cousseau, J.; Trichet, L.; Rouxel, J. *Bull. Soc. Chim. Fr.* **1973**, 872−878.
(74) Tomas, A.; Guittard, M.; Chevalier, R.; Flahaut, J. *C. R. Seances Acad. Sci., Ser. C* **1976**, *282*, 587−589.
(75) Lafond, A.; Cario, L.; van der Lee, A.; Meerschaut, A. *J. Solid State Chem.* **1996**, *127*, 295−301.
(76) Meerschaut, A.; Lafond, A.; Hoistad, L. M.; Rouxel, J. *J. Solid State Chem.* **1994**, *111*, 276−282.
(77) Takahashi, T.; Ametani, K.; Yamada, O. *J. Cryst. Growth* **1974**, *24/25*, 151−153.
(78) Jeitschko, W.; Donohue, P. C. *Acta Crystallogr., Sect. B: Struct. Crystallogr. Cryst. Chem.* **1975**, *31*, 1890−1895.
(79) Donohue, P. C.; Jeitschko, W. *Mater. Res. Bull.* **1974**, *9*, 1333−1336.
(80) Moseley, P. T.; Brown, D.; Whittaker, B. *Acta Crystallogr.* **1972**, *B28*, 1816−1821.
(81) Besrest, F.; Collin, G. *J. Solid State Chem.* **1977**, *21*, 161−170.
(82) Besrest, F.; Collin, G. *J. Solid State Chem.* **1978**, *24*, 301−309.
(83) Collin, G.; Barthélémy, É.; Gorochov, O. *C. R. Seances Acad. Sci., Ser. C* **1973**, *277*, 775−778.
(84) Plumier, R.; Sougi, M.; Collin, G. *Solid State Commun.* **1974**, *14*, 971−973.
(85) Plumier, R.; Sougi, M.; Lecomte, M. *J. Appl. Phys.* **1981**, *52*, 2320−2322.
(86) Plumier, R.; Sougi, M.; Lecomte, M.; Collin, G. *Phys. Lett. A* **1979**, *74*, 354−356.
(87) Plumier, R.; Sougi, M.; Lecomte, M.; Collin, G. *J. Magn. Magn. Mater.* **1980**, *15−18*, 509−511.
(88) Guseinov, G. G.; Gasymov, V. A.; Aliev, I. P.; Mamedov, K. S. *Inorg. Mater. (Transl. of Neorg. Mater.)* **1981**, *17*, 556−558.
(89) Tougait, O.; Ibers, J. A. *Inorg. Chem.* **2000**, *39*, 1790−1794.
(90) Rodier, N.; Tien, V. *Acta Crystallogr., Sect. B: Struct. Crystallogr. Cryst. Chem.* **1976**, *32*, 2705−2707.
(91) Rustamov, P. G.; Kurbanov, T. K.; Aliev, O. M.; Aliev, I. P. *Inorg. Mater. (Transl. of Neorg. Mater.)* **1984**, *20*, 1664−1667.
(92) Adolphe, C.; Laruelle, P. *Bull. Soc. Fr. Mineral. Cristallogr.* **1968**, *91*, 219−232.
(93) Adolphe, C. *Ann. Chim. (Paris)* **1965**, *10*, 271−297.
(94) Tomas, A.; Robert, M.; Adolphe, C.; Guittard, M. *Mater. Res. Bull.* **1984**, *19*, 1643−1646.
(95) Souleau, C.; Guittard, M.; Wintenberger, M. *Bull. Soc. Chim. Fr.* **1966**, 1644−1645.
(96) Agaev, A. B.; Aliev, V. O.; Aliev, O. M. *Russ. J. Inorg. Chem. (Transl. of Zh. Neorg. Khim.)* **1996**, *41*, 306−312.
(97) Collin, G.; Flahaut, J. *J. Solid State Chem.* **1974**, *9*, 352−357.
(98) Balz, D.; Plieth, K. *Z. Elektrochem.* **1955**, *59*, 545−551.
(99) Huang, F. Q.; Ibers, J. A. *J. Solid State Chem.* **2001**, *159*, 186−190.
(100) Pell, M. A.; Ibers, J. A. *Chem. Ber.* **1997**, *130*, 1−8.
(101) Cody, J. A.; Ibers, J. A. *Inorg. Chem.* **1995**, *34*, 3165−3172.
(102) Brese, N. E.; Ibers, J. A. *J. Solid State Chem.* **1988**, *76*, 1−6.
(103) Tomas, A.; Rigoult, J.; Guittard, M.; Pierre, L. *Acta Crystallogr., Sect. B: (Struct. Crystallogr. Cryst. Chem.* **1980**, *36*, 1987−1989.
(104) Chaqour, S. M.; Tomas, A.; Lemoine, P. *Acta Crystallogr., Sect. C: (Cryst. Struct. Commun.* **1994**, *50*, 1655−1657.
(105) Einullaev, A. V.; Mamedov, N. V.; Sadykhov, R. Z.; Agaev, A. B. *Inorg. Mater. (Transl. of Neorg. Mater.)* **2000**, *36*, 6−7.
(106) Bronger, W.; Miessen, H.-J.; Schmitz, D. *J. Less-Common Met.* **1983**, *95*, 275−282.
(107) Litteer, J. B.; Sirchio, S. A.; Fettinger, J. C.; Smolyaninova, V.; Eichhorn, B. W.; Greene, R. L. *Chem. Mater.* **1999**, *11*, 1179−1182.
(108) Collin, G.; Laruelle, P. *Acta Crystallogr., Sect. B: (Struct. Crystallogr. Cryst. Chem.* **1974**, *30*, 1134−1139.
(109) Cenzual, K.; Gelato, L. M.; Penzo, M.; Parthé, E. *Z. Kristallogr.* **1990**, *193*, 217−242.
(110) Lu, Y.-J.; Ibers, J. A. *Comments Inorg. Chem.* **1993**, *14*, 229−243.
(111) Huang, F. Q.; Mitchell, K.; Ibers, J. A. *Inorg. Chem.* **2001**, *40*, 5123−5126.
(112) Cody, J. A.; Mansuetto, M. F.; Chien, S.; Ibers, J. A. *Mater. Sci. Forum* **1994**, *152−153*, 35−42.
(113) Kanatzidis, M. G.; Sutorik, A. C. *Prog. Inorg. Chem.* **1995**, *43*, 151−265.
(114) Tulsky, E. G.; Long, J. R. *Chem. Mater.* **2001**, *13*, 1149−1166.
(115) Brennan, T. D.; Ibers, J. A. *J. Solid State Chem.* **1992**, *97*, 377−382.
(116) Basançon, P.; Adolphe, C.; Flahaut, J.; Laruelle, P. *Mater. Res. Bull.* **1969**, *4*, 227−238.
(117) Sutorik, A. C.; Albritton-Thomas, J.; Hogan, T.; Kannewurf, C. R.; Kanatzidis, M. G. *Chem. Mater.* **1996**, *8*, 751−761.
(118) Mansuetto, M. F.; Keane, P. M.; Ibers, J. A. *J. Solid State Chem.* **1992**, *101*, 257−264.
(119) Wu, P.; Christuk, A. E.; Ibers, J. A. *J. Solid State Chem.* **1994**, *110*, 337−344.
(120) Huang, F. Q.; Choe, W.; Lee, S.; Chu, J. S. *Chem. Mater.* **1998**, *10*, 1320−1326.
(121) Wu, P.; Ibers, J. A. *J. Solid State Chem.* **1994**, *110*, 156−161.
(122) Patschke, R.; Heising, J.; Kanatzidis, M. *Chem. Mater.* **1998**, *10*, 695−697.
(123) Norling, B. K.; Steinfink, H. *Inorg. Chem.* **1966**, *5*, 1488−1491.
(124) Stoll, P.; Dürichen, P.; Näther, C.; Bensch, W. *Z. Anorg. Allg. Chem.* **1998**, *624*, 1807−1810.
(125) Huang, F. Q.; Ibers, J. A. *J. Solid State Chem.* **2001**, *158*, 299−306.
(126) Huang, F. Q.; Ibers, J. A. *J. Solid State Chem.* **2000**, *151*, 317−322.
(127) Sutorik, A. C.; Albritton-Thomas, J.; Kannewurf, C. R.; Kanatzidis, M. G. *J. Am. Chem. Soc.* **1994**, *116*, 7706−7713.
(128) Brechtel, E.; Cordier, G.; Schäfer, H. *Z. Naturforsch., B: Anorg. Chem., Org. Chem.* **1980**, *35*, 1−3.
(129) Patschke, R.; Brazis, P.; Kannewurf, C. R.; Kanatzidis, M. *Inorg. Chem.* **1998**, *37*, 6562−6563.
(130) Patschke, R.; Brazis, P.; Kannewurf, C. R.; Kanatzidis, M. *J. Mater. Chem.* **1998**, *8*, 2587−2589.
(131) Klawitter, Y.; Näther, C.; Jess, I.; Bensch, W.; Kanatzidis, M. G. *Solid State Sciences* **1999**, *1*, 421−431.
(132) Bensch, W.; Dürichen, P. *Chem. Ber.* **1996**, *129*, 1489−1492.
(133) Krönert, W.; Plieth, K. *Z. Anorg. Allg. Chem.* **1965**, *336*, 207−218.
(134) Cody, J. A.; Ibers, J. A. *Inorg. Chem.* **1996**, *35*, 3836−3838.
(135) Wu, P.; Ibers, J. A. *Z. Kristallogr.* **1993**, *208*, 35−41.
(136) Flahaut, J.; Laruelle, P. In *The Chemistry of Extended Defects in Non-Metallic Solids*; Eyring, L., O'Keeffe, M., Eds.; North-Holland Publishing Co.: London, 1970; pp 109−123.
(137) de Saint-Giniez, D.; Laruelle, P.; Flahaut, J. *C. R. Seances Acad. Sci., Ser. C* **1968**, *267*, 1029−1032.
(138) Hwu, S.-J.; Bucher, C. K.; Carpenter, J. D.; Taylor, S. P. *Inorg. Chem.* **1995**, *34*, 1979−1980.
(139) Lin, S.-H.; Mao, J.-G.; Guo, G.-C.; Huang, J.-S. *J. Alloys Compd.* **1997**, *252*, L8−L11.
(140) Huang, F. Q.; Ibers, J. A. *Acta Crystallogr., Sect. C: Cryst. Struct. Commun.* **1999**, *55*, 1210−1212.
(141) Nanjundaswamy, K. S.; Gopalakrishnan, J. *J. Solid State Chem.* **1983**, *49*, 51−58.
(142) Plumier, R.; Lecomte, M.; Collin, G.; Keller-Besrest, F. *Phys. Lett. A* **1980**, *76*, 419−420.
(143) Yang, Y.; Ibers, J. A. *J. Solid State Chem.* **2000**, *149*, 384−390.
(144) Huang, F. Q.; Ibers, J. A. *J. Solid State Chem.* **2001**, *160*, 409−414.
(145) Tougait, O.; Ibers, J. A. *Inorg. Chem.* **2000**, *39*, 6136−6138.
(146) Mujica, C.; Llanos, J.; Peters, K.; Peters, E.-M.; von Schnering, H. G. *Z. Kristallogr.-New Cryst. Struct.* **1998**, *213*, 458.
(147) Llanos, J.; Mujica, C.; Wittke, O.; Gómez-Romero, P.; Ramírez, R. *J. Solid State Chem.* **1997**, *128*, 62−65.

CR010319H